TWRI TR-186

Quality and Membrane Treatability of the Lake Houston Water Supply

Final Report

October 1, 2001

By

Shankar Chellam,
Ramesh Sharma,
Grishma Shetty (all with the University of Houston),
and
Ying Wei (City of Houston)

PUBLISHED BY
THE TEXAS WATER RESOURCES INSTITUE
(TWRI)

Quality and Membrane Treatability of the Lake Houston Water Supply

by

Shankar Chellam, Ramesh Sharma, and Grishma Shetty, Civil Engineering Department, the University of Houston, Houston, TX,
and
Ying Wei, City of Houston

March 2000 to August 2001
Grant Number HQ-96-GR-02700-UH-002.

Research on which this report was based was financed, in part, by the U.S. Department of the Interior and the U.S. Geological Survey, through the Texas Water Resources Institute (TWRI).

Technical Report 186
Texas Water Resources Institute
Texas A&M University
College Station, TX 77843-2118

October 2001

1. PROBLEM AND RESEARCH OBJECTIVES

1.1. Statement of Need

Currently, sections of Harris and Montgomery counties located North and Northeast of Houston use groundwater almost exclusively. These areas have witnessed substantial population growth and associated increases in water demand. In 1999 approximately 60% of potable water in Houston and its adjoining communities was produced from surface water. The remaining approximately 40% was derived from groundwater. However, the "Subsidence District" which is the authority responsible for granting groundwater permits has mandated that groundwater use needs to be decreased to 20% within the next few years so as to limit subsidence.

Pipelines are not available to distribute purified water from the existing surface water treatment plants located in the South and East of Houston to the Northern areas that actually require additional water. Because Lake Houston is located in the geographical area of interest and is a surface water source, the City of Houston is interested in developing it for its future water needs. Additionally, a favorable hydraulic gradient exists from the Lake to the proposed service areas in Harris and Montgomery counties.

Federal regulations such as the Stage II of the Disinfectant/Disinfection By-Products Rule (1) and the Enhanced Surface Water Treatment Rule (2) are expected to be promulgated in the near future. These rules are anticipated to introduce more stringent maximum contaminant levels (MCLs) for total trihalomethanes (THMs) and haloacetic acids (HAAs), possibly introduce new MCLs for individual species of THMs and HAAs, reduce turbidity levels, and enhance inactivation/removal requirements for *Cryptosporidium*. (*Cryptosporidium* was the causative protozoan for the more than 400,000 cases of acute gastrointestinal disease in Milwaukee, WI in March 1993.) The treatment processes in the City of Houston's existing water purification plants are not expected to be sufficient in meeting these anticipated regulations.

Therefore, both regulatory requirements and engineering considerations point towards Lake Houston as an attractive surface water source for the next water purification plant to supply potable water to the City and its adjoining communities. However, water quality in Lake Houston can be characterized as being poor with high concentrations of turbidity, color, total organic carbon (TOC), nutrients such as phosphorus and nitrogen, etc. (3).

Pressure-driven membrane processes can be employed as effective barriers against a wide range of contaminants including particles, turbidity, protozoan cysts and oocysts, bacteria, viruses, color, organic carbon, disinfection by-product (DBP) precursors, and dissolved metals. Additionally, microfiltration (MF) and ultrafiltration (UF) pretreatment may be necessary to reduce fouling rates and increase chemical cleaning intervals during surface water nanofiltration (NF) (4). Therefore, an integrated membrane system employing MF or UF pretreatment to NF is expected to be an important treatment candidate for Lake Houston water.

Nanofiltration (NF) membranes typically operate at pressures less than 100 psi and are capable of high rejections of natural organic matter (NOM) and precursors to disinfection by-products (DBP) including trihalomethanes (THMs) and haloacetic acids (HAAs) (5-8), many of which are suspected carcinogens, mutagens, or teratogens.

1.2. Previous Research on Nanofilter Permeate Water Quality

NF permeate water quality in multi-solute systems typical of water treatment applications is a complex function of physicochemical (steric and electrostatic) interactions between the membrane and dissolved solutes and many other factors that influence the solubility and diffusivity of solutes and water in the membrane phase (9). Even though many attempts have been made to describe solute transport across NF membranes from first principles, models are not available yet to accurately predict rejection from multi-component systems. This is due in part to complications arising from the need to preserve

electroneutrality, ion pairing and coupling (10), and changes in diffusivity and viscosity in mixed solute systems.

One method of modeling ion coupling in multi-solute systems involves relating the separation data for a reference electrolyte such as NaCl to the target solute under consideration (11). At the heart of this approach is the measurement of a parameter $(-\Delta\Delta G/RT)_{ion}$ that is interpreted as the free energy required to bring the ion from the bulk solution to the inter-phase region of the membrane. In principle, if $(-\Delta\Delta G/RT)_{ion}$ values for all species in solution are known along with their diffusion and dissociation data at a fixed temperature, it will be possible to calculate solute permeability in multi-component systems. However, in most applications the complete feed water composition is not known. Additionally, thermodynamic properties of NOM cannot be well estimated because it is heterogeneous and does not possess a well-defined chemical and structural formula. For these reasons, a useful free energy based model may never be developed for NOM removal during water treatment. Therefore, our current approach to determining NF selectivity to NOM, DBP precursors, and inorganic ions in multi-component systems is largely empirical and is based on site-specific experiments (4-6, 8).

In order to better protect public health, the U.S. Environmental Protection Agency (EPA) is facilitating regulatory negotiations to possibly reduce maximum contaminant levels (MCLs) of total THMs[1] (TTHMs), HAA5[2], and possibly introduce new ones for HAA9[3], total organic halide (TOX), and even individual THM and HAA species under the Disinfectant/DBP (D/DBP) rule (1). Earlier regulatory negotiations to reach consensus on the control of microbial contaminants and DBPs in drinking water resulted in the promulgation of the Information Collection Rule (ICR). The ICR required certain municipalities (based on population served and influent total organic carbon (TOC) concentration) to conduct experiments using NF or granular activated carbon to better assess their feasibility to reduce DBP precursors under conditions close to those in a full-scale plant in terms of feed water quality and operational parameters (12).

Hindered transport across membrane pores controls the transport of single neutral solutes across cellulose acetate NF membranes (13). Molecular size correlates well with the retention of single organic solutes by commercial NF membranes even though molecular charge and polarity also influenced rejection (14). In contrast to the single solutes of known properties employed in much previous research on organics separation by NF, NOM is inherently heterogeneous and possesses a wide distribution of molecular weight, aromaticity, functionality, hydrophobicity, and reactivity (15-17). Additionally, membrane-NOM interactions depend on solution chemistry parameters including background ionic strength, pH, and concentrations of multivalent ions (e.g. Ca^{+2}, Al^{+3}, Fe^{+3}) (18, 19). Because complete chemical compositions of feed waters are often not available and since NOM is inherently heterogeneous, models based on NOM and membrane thermodynamic properties may never accurately predict its rejection from natural and pretreated waters by NF. We circumvent some of these difficulties by taking a lumped parameter approach to mass transfer calculations from multi-solute systems encountered during water treatment.

Previous NF studies on Florida groundwaters have suggested that physical sieving is the dominant mechanism for NOM and THM and HAA precursor rejection (6). However, recent evidence appears to suggest that molecular diffusion also plays an important role in the transport of these contaminants across new generation thin film composite (TFC) NF membranes formulated specifically for organics removal (5, 7). No models (including those developed by manufacturers themselves) currently exist to quantify rejection of NOM and DBP precursors by these membranes. Such a model will allow better design of pilot-scale experiments and more thorough interpretation of site-specific permeate water quality data from

[1] TTHM denotes the sum of concentrations of chloroform, chlorodibromo methane, dichlorobromo methane, and bromoform.

[2] HAA5 denotes the sum of concentrations of monochloro-, dichloro-, trichloro-, monobromo-, and dibromo acetic acid.

[3] HAA9 denotes the sum of HAA5 and concentrations of bromochloro-, dibromochloro-, dichlorobromo-, and tribromo acetic acid.

pilot studies conducted by municipalities to obtain design parameters for NF plants in anticipation of federal regulations establishing more stringent MCLs for THMs and HAAs.

1.3. Goals and Objectives

Scale-up techniques for membrane systems employed for water treatment in terms of fouling or water quality has not yet been identified necessitating long pilot-studies in support of design. One of the primary objectives of this work is to investigate fundamental approaches in determining scale-up procedures for permeate water quality obtained from nanofiltration membranes.

This report summarizes results from several crossflow nanofiltration experiments that appear to demonstrate diffusion-limited rejection of model organics, natural organic matter, as well as trihalomethane, and haloacetic acid precursors. Most previous studies have not reported rejection of precursors to all nine haloacetic acids containing chlorine and bromine by NF for because until recently stable calibration standards for dibromochloro-, dichlorobromo-, and tribromo acetic acid were not available.

We develop and verify a simple closed form expression for contaminant rejection from Lake Houston surface water based on the homogenous solution diffusion model (HSDM) (20) under conditions typical of water treatment NF applications using commercially available thin film composite membranes. Solute permeation and back-diffusion mass transfer coefficients are used to fit this model to rejection of several organic contaminants important in water treatment including dissolved organic carbon (DOC), ultraviolet absorption at 254 nm and one cm path length (UV_{254}), and precursors to TTHM, HAA9, and other DBPs.

We also investigate possible changes in reactivity of natural organic matter (NOM) following NF. Relationships between dissolved organic carbon, UV_{254}, chlorine consumption, trihalomethanes, and haloacetic acids, in chlorinated NF feed and permeate waters are established. Universalities in trihalomethane and haloacetic acid formation and speciation are also explored with particular emphasis on the extent of bromine incorporation, bromide utilization and formation of currently unregulated mixed bromochloro haloacetic acid species.

2. METHODOLOGY

2.1. Development of an Integral Model for Permeate Water Quality

A recently developed general model including concentrate recycle (21) will be described in this section even though recycling was not employed in our experiments. This is done because many U.S. EPA mandated information collection rule studies for regulatory compliance have employed concentrate recycle (also referred to as feed and bleed mode) (7, 21). Thus, to apply the model derived herein to the experimental data generated during this study, the recycle flow should be set equal to zero. Consider a NF system operating in the feed and bleed mode (Figure 2.1).

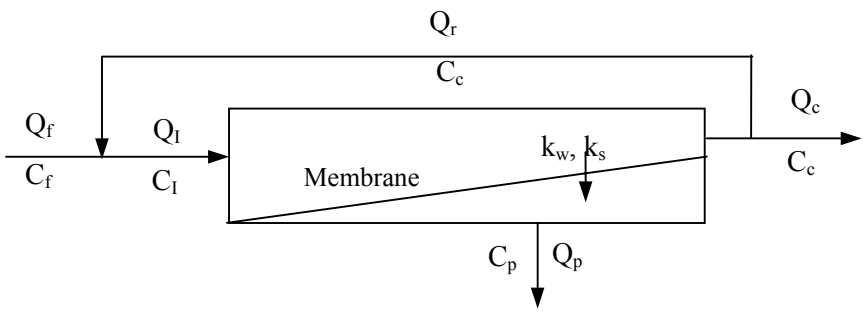

Figure 2.1. Schematic diagram of a crossflow NF system operated in the feed and bleed mode.

In this configuration, a portion of the reject water is recirculated to maintain a predetermined tangential velocity (or shear rate) to limit concentration polarization. At steady state the volumetric water (J_w) and solute (J_s) fluxes when transport is diffusion-dominated and coupling is negligible (assuming constant membrane properties and diffusivity) is (9, 11, 20, 22):

$$J_w = k_w \Delta P = \frac{Q_p}{A} \tag{1}$$

$$J_s = k_s \Delta C = J_w C_p \tag{2}$$

Where k_w, k_s, Q_p and C_p represents a membrane constant, solute permeation coefficient, permeate flow, and permeate concentration, respectively. ΔP and ΔC are the driving forces for water and solute transport and are equal to net pressure (including osmotic pressure) and concentration differential between the membrane and permeate values. Fundamentally, the membrane constant k_w is related to the water diffusion coefficient in the polymeric membrane phase D_w, its concentration in the membrane c_w, its partial molar volume v_w, the universal gas constant $\boldsymbol{R}$, the absolute temperature T, and the membrane thickness Δx as (23):

$$k_w = \frac{D_w c_w v_w}{\boldsymbol{R} T \Delta x} \tag{3}$$

Similarly, the solute permeation coefficient is related to its diffusivity in the membrane D_s and its distribution (partition) coefficient K_s as:

$$k_s = \frac{D_s K_s}{\Delta x} \tag{4}$$

Because many thermodynamic parameters in Equations 3 and 4 are not known for commercial membranes, we treat k_w and k_s as lumped parameters and will estimate them from experimental permeate flux and solute rejection data. These equations were originally developed to model mass transfer of simple electrolytes and organics across non-porous (dense) membranes. However, its applicability for NOM rejection by NF membranes especially in multi-solute systems has not yet been evaluated. The feed water (R_f) and element (R_e) recoveries are defined as:

$$R_f = \frac{Q_p}{Q_f} \text{ and } R_e = \frac{Q_p}{Q_f + Q_r} \tag{5}$$

Where Q_f and Q_r denote the feed and recycle flows respectively. At steady state, a mass balance around the membrane module gives the reject concentration C_c:

$$C_c = \frac{C_f - R_f C_p}{1 - R_f} \tag{6}$$

Recycling part of the reject water to the feed side increases both the crossflow velocity as well as the influent concentration (C_I). At steady state, the influent concentration to the membrane is the flow weighted average of the concentrations in the recycle and feed streams. Therefore, from Equations 5 and 6 we get:

$$C_I = \left(\frac{R_e}{R_f}\right) C_f + \left(1 - \frac{R_e}{R_f}\right)\left(\frac{C_f - R_f C_p}{1 - R_f}\right) \tag{7}$$

The ratio C_l/C_f is interpreted as a concentration factor that $\rightarrow 1$ as $R_e \rightarrow R_f$ ($Q_r \rightarrow 0$). A simple one dimensional description of concentration polarization based on film theory in which the net flux of solute in the boundary layer is equated to the flux through the membrane results in (11, 22, 24):

$$\frac{C_m - C_p}{C_b - C_p} = \exp\left(\frac{J_w}{k_b}\right) \tag{8}$$

Where C_m is the concentration near the membrane surface, C_b is the bulk solution concentration, and k_b is the solute back-transport mass transfer coefficient. Approximating C_b as an arithmetic average of the influent and reject concentrations, the change in concentration across the membrane from Eq. 8 becomes:

$$\Delta C = C_m - C_p = \left(\frac{C_I + C_c}{2} - C_p\right)\exp\left(\frac{J_w}{k_b}\right) \tag{9}$$

Combining Eqns. 1, 2, 7, and 9 a closed form analytical expression for the solute rejection R is obtained:

$$R = 1 - \frac{C_p}{C_f} = 1 - \frac{k_s \exp\left(\frac{J_w}{k_b}\right)}{k_s \exp\left(\frac{J_w}{k_b}\right) + \frac{2J_w(1-R_f)}{2-R_e}} \tag{10}$$

Equation 10 represents a solute mass transfer model for systems employing concentrate recycle that considers the entire membrane element as having constant bulk solution concentration calculated as the average of the influent and reject concentrations. Therefore, it represents an important approximation whose accuracy increases as the feed water recovery decreases (so as to limit increases in C_b). However, invoking this approximation results in an analytical, closed form solution thereby lending itself to mechanistic interpretation of solute rejection data from multi-component feed waters obtained during municipal water treatment experiments conducted in support of plant design and/or trouble shooting. One method of calculating k_s and k_b is by using appropriate mass transfer correlations (25). These empirical correlations are intimately linked to the geometry and type of spacer material used as well as the local hydrodynamics and typically do not include changes in viscosity and diffusivity caused by concentration polarization. Because spacer information is proprietary and hydrodynamic behavior in the presence of spacers are not well understood, k_s and k_b will be estimated from experimental data in this study as described in the next section.

Because the partial derivative of R with respect to R_f in Equation 10 is always negative, it can be concluded that rejection will decrease with increasing recovery. Mechanistically, this occurs because of increasing concentration gradient thereby increasing the driving force for solute permeation across the membrane. This behavior will be employed predominantly to study solute rejection by NF membranes in this report.

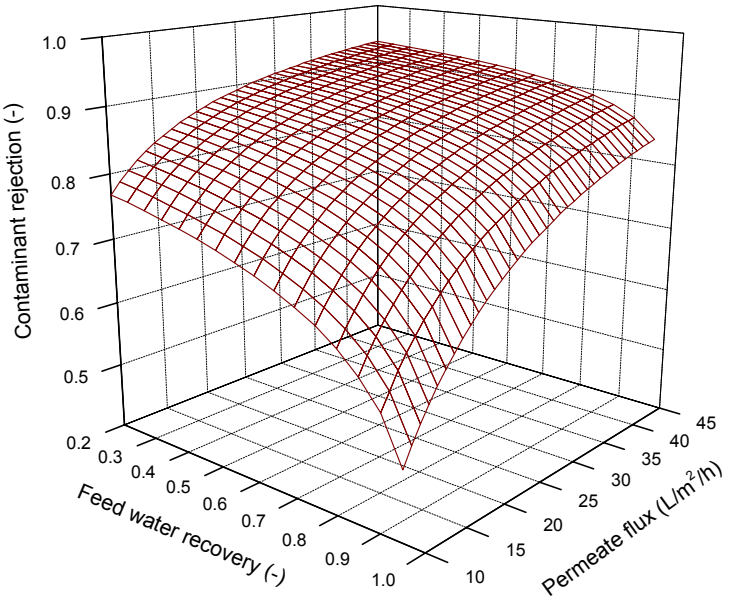

Figure 2.2. Model Predictions of changes in contaminant removal with flux and recovery.

Figures 2.2 depicts contaminant removal as a function of feed water recovery and permeate flux for one arbitrary combination of permeation coefficient and back-transport coefficient. Rejection decreases as recovery increases because the concentration gradient across the membrane is increased. Rejection effectively increases with permeate flux according to the HSDM because increasing transmembrane pressure does not influence solute transport while increasing permeate flux (23, 26, 27).

2.2. Estimation of Mass Transfer Coefficients

The Levenberg-Marquardt algorithm (28) was employed to minimize the sum of squares of the residuals for all data points (error sum of squares (S)) to determine k_s and k_b. Estimates for selected datasets were also verified using a more robust full Newton-type method to minimize the nonlinear sum of squares employing an analytical Jacobian (29). The joint (1-α) likelihood region for k_s and k_b corresponds to the contour with level:

$$S_F = S\left(\hat{\Theta}\right)\left[1 + \frac{pF(p, n-p, \alpha)}{n-p}\right] \tag{11}$$

Where α is the significance level, S_F denotes the value of the sum of squares contour defining the (1-α) region, S is the sum of squares of the residuals, $\hat{\Theta}$ denotes the optimal parameter estimate, p is the number of parameters (p=2 in Equation 10), n is the number of observations, F(p,n-p,α) is the cumulative Fisher F distribution corresponding to significance level α with p and n-p degrees of freedom for the numerator and denominator respectively. Nonlinear nominal likelihood intervals and nonlinear behavior were quantified by profiling (30, 31). The profile t function is defined as:

$$\hat{o}(\Theta_p) = \text{sign}\left(\Theta_p - \hat{\Theta}_p\right)\frac{\sqrt{\tilde{S}(\Theta_p) - S(\hat{\Theta})}}{s} \tag{12}$$

Where Θ_p denotes a parameter, $\hat{\Theta}_p$ denotes the parameter's optimal value, $\tilde{S}$ is the profile sum of squares function, and s is the standard deviation estimated as $S(\hat{\Theta})/(n-p)$. Plots of the profile t function τ versus the studentitized parameter δ (Eq. 13) provide exact likelihood intervals for k_s and k_b.

$$\delta(\Theta_p) = \frac{\Theta_p - \hat{\Theta}_p}{se(\hat{\Theta}_p)} \quad (13)$$

Where, $se(\hat{\Theta}_p)$ denotes the standard error of the least square estimate. Likelihood profile traces of $\tilde{k}_b$ on k_s and $\tilde{k}_s$ on k_b were also generated to determine the extent of non-linearity in parameter estimation.

2.3. Calculation of Aqueous Diffusion Coefficients

The method proposed by Hayduk and Laudie was used to calculate the aqueous diffusion coefficient of dilute polyethylene glycol solutions of different molecular weights (32) because of its computational simplicity. The temperature dependence is not explicit because it needs to be incorporated into the viscosity term. The Hayduk and Laudie method is based on Equation 14:

$$D_{BW} = \frac{13.26 \times 10^{-5}}{\varsigma_w^{1.14} V_B^{0.589}} \quad (14)$$

Where,
D_{BW} = diffusivity of species (cm^2/s)
ϕ_w = solvent association factor (2.26 for water)
MW = molecular weight of solvent (18 g/mol for water)
T = temperature (293 K)
V_B = atomic volume increment (cm^3/mol)
η_w = solution viscosity (0.93 cP for water)

2.4. Experimental Work

2.4.1. Analytical Methods

To ensure the integrity of the experimental program, only EPA approved and/or Standard Methods for sampling, sample preparation and analyses were employed. All samples taken to the City of Houston laboratory (for DBP precursor and anion analyses) were appropriately labeled and documented in a logbook. In addition, samples were refrigerated at 4°C after collection and were analyzed within 15 days of sampling. A detailed description of water quality analyses is given next.

2.4.1.1. Nanopure Water System

All synthetic water experiments as well as chemical analyses were carried out using nanopure water produced from commercial laboratory scale system (Max159 Modulab®, U.S. Filter Corporation, Lowell, MA). The system consisted of multi-staged treatment to remove microbial, ionic, organic, and particulate contaminants. Activated carbon filter (DICR 1000-4, US Filter Corporation, Lowell, MA) was installed upstream of a RO membrane (AK 139 ROMA, Water Equipment Technology, West Palm Beach, FL). Trace organics were removed using UV irradiation (UV8100, US Filter Corporation, Lowell, MA) in conjunction with an organic cartridge filter (DIOR 1000-4, US Filter Corporation, Lowell, MA). Two mixed bed ion exchange resins (DIMN 1000-4, US Filter Corporation, Lowell, MA) were employed to remove the remaining inorganics. Finally, a 0.22 μm filter (FCCFE 1452, US Filter Corporation, Lowell, MA) was utilized for particle and microorganism removal. Modulab Analytical systems was designed to purify water up to 18.30 mega ohm-cm resistivity and dissolved organic carbon concentration < 3 μg/L.

2.4.1.2. pH

The pH was measured using a pH meter (model 320, Orion Research Inc., Beverly, MA). The meter was calibrated at pH 4 and 7 using phthalate (SB 98-500, Fisher Scientific, Houston, TX) and phosphate (SB

108-500, Fisher Scientific, Houston, TX) buffers. Analyses were performed immediately after sample collection.

2.4.1.3. Conductivity

Conductivity was measured using a probe (cell-013005D, Orion Research Inc., Beverly, MA) connected to a conductance meter (model 125, Orion Research Inc., Beverly, MA). Calibration with NaCl standards, 1413 μS/cm (011007 Orion Research Inc., Beverly, MA) and 12.9 mS/cm (011006 Orion Research Inc., Beverly, MA) resulted in a cell constant of 0.48/cm. The conductivity meter automatically compensated for the temperature changes using temperature coefficient for NaCl (2.1%/°C). Analyses were performed immediately upon sample collection.

2.4.1.4. Sodium

Sodium was measured using atomic absorption spectroscopy (300AA-Perkin Elmer, Norwalk, CA). A hollow cathode lamp was used with a lamp current of 8 mA. Sodium emission was measured at a wavelength of 320.3 nm with a slit width of 0.7 nm using a burner head of 10 cm. The instrument was warmed up for 20-30 minutes to stabilize the energy source. Standards were prepared by diluting 1,000 mg/L stock solution of NaCl. Standard solutions corresponding to 5, 10, 15, 20, 30, 40, 50 and 75 mg Na^+/L were prepared to encompass the expected metal concentration in samples after appropriate dilutions. A typical sodium calibration curve obtained in this study is shown in Figure 2.3.

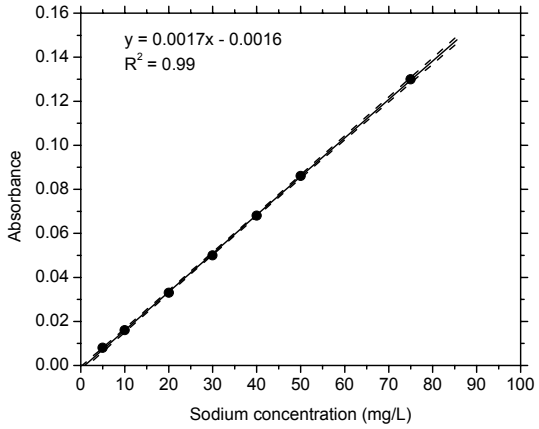

Figure 2.3. A typical calibration curve for sodium analysis using atomic absorption spectroscopy. The solid line denotes the best fit ; the dashed lines represent the 95% confidence intervals of the mean of the observations.

2.4.1.5. Dissolved Organic Carbon

Combustion infrared method (SM 5310 B) employing a Shimadzu 5050TOC analyzer (Columbia, MD) was used for DOC analysis. Samples were collected in amber colored bottles that had been heated at 550 ºC for 5 h and cooled to room temperature prior to use. Preheating at 550 ºC was necessary to ensure organic free bottles. These bottles were sealed with Teflon–lined caps, stored at 4 ºC, and analyzed within 7 days. Stock solution (100 mg DOC /L) was made using potassium hydrogen phthalate ($C_8H_5O_4K$, Nacalai Tesque, Kyoto, Japan). To standardize the TOC analyzer, standard solutions corresponding to 0.5, 1, 2, 4, 6, 8 and 10 mg/L were made with appropriate dilutions using nanopure water. Figure 2.4 shows one typical calibration curve obtained in this study for DOC measurement.

Various instrument cleaning cycles were run prior to sample analyses. Three blank solutions (nanopure water) were used to establish a baseline reading. The DOC analyzer was calibrated every time the machine was switched on using 0.5, 1, 2, 4, 6, 8, and 10 mg/L DOC standards. A fresh stock solution of the standards was prepared every month to ensure accurate calibration. In order to analyze the

background and carryover effects, blank samples were run at regular intervals during the analyses. Concentrated phosphoric acid was used to adjust sample pH to 2. Carrier gas designated as "ultra zero" (UZCA-310 Matheson-Trigas, Carbon content <0.1%) was employed. DOC was measured by injecting the acidified and oxygen purged (carbon dioxide stripped) sample to DOC analyzer through Auto sampler (ASI, 5000 Shimadzu).

All results reported here are an average of maximum of five injections (three measurements were selected from five so as to get coefficient of variation (CV) less than 2%, where CV is calculated as standard deviation divided by mean).

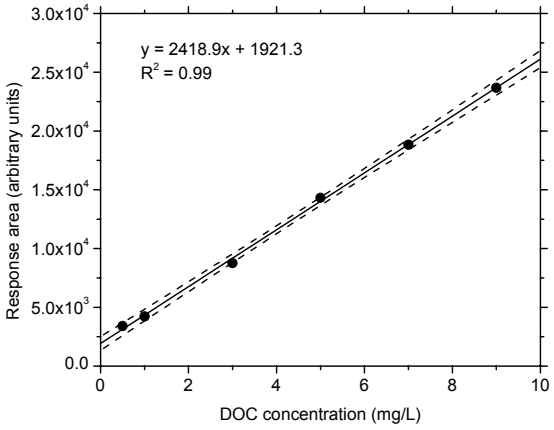

Figure 2.4. A typical calibration curve for DOC measurements. The solid line denotes the best fit whereas the dashed lines represent the 95% confidence intervals of the mean of the observations.

2.4.1.6. UV Absorbance at 254 nm

A DR/4000 spectrometer (Hach Company, Loveland CO) was employed to measure absorbance at 254 nm. A 1 cm quartz cell (48228-00, Hach Company, Loveland CO) was rinsed several times with organic free water and wiped thoroughly before zeroing the instrument. Samples were prefiltered using a 0.45 μm filter to avoid interference from suspended particulates. After zeroing the instrument, the cell containing sample was placed in cell holder. All absorbance values reported in this study have been normalized to 1 cm path length.

2.4.1.7. Anions

Determination of inorganic anions was carried out in accordance with EPA method 300.1 (33). Anions analyzed using this method include bromide, chlorite, chlorate, chloride, fluoride, nitrate, nitrite, orthophosphate, and sulfate. The anions of interest were separated and measured, using anion chromatography system (DX 500, Dionex Corporation, Sunnyvale, CA) comprising of a guard column, analytical column (Dionex AG9-HC), suppressor device, and a conductivity detector (Dionex CD 20). Eluent used was 9.0 mM Na_2CO_3. A typical calibration curve obtained for chloride ion measurement is shown in Figure 2.5.

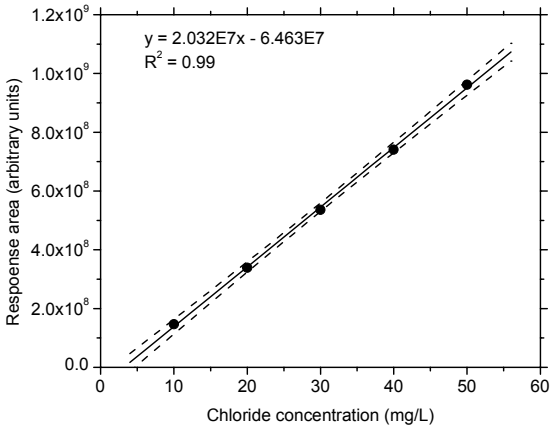

Figure 2.5. Typical calibration curve for chloride ion measurement using ion chromatography. The solid line denotes the best fit whereas the dashed lines represent the 95% confidence intervals of the mean of the observations.

2.4.1.8. Hardness

Calcium hardness was determined in accordance with standard method (SM 3500 C) employing EDTA (0.01M) titration with Erichrom black T as an indicator. pH of the samples were raised to 12 in order to precipitate magnesium using 1.0 M NaOH prior to titration.

2.4.1.9. Alkalinity

In performing the alkalinity measurements, acid (0.02N H_2SO_4) was added in appropriate increments and pH was recorded after addition of each aliquot to the well-mixed sample. Titration was continued up to pH 3-3.5. Inflection points of these titration curve were determined to obtain the end points of titration. Alkalinity values were calculated using the equivalents of acid required to reach the end point and are reported as mg/L as $CaCO_3$.

2.4.1.10. Free Chlorine

Free chlorine was measured using DR/4000 procedure (Hach program–1450) employing AccuVac method. This procedure is equivalent to USEPA method 330.5 and SM 4500-Cl G for drinking water. The estimated detection limit is 0.01 mg/L. This method is applicable only in the range of 0-2 mg/L of free chlorine. For solutions having higher free chlorine concentrations appropriate dilution were made.

2.4.1.11. Ammonia

Ammonia was measured as per SM 4500 –NH_3 C employing nesslerization method at a wavelength of 425 nm. The range of ammonia concentration using this method is 0.4-5 mg/L. The ammonia concentrations observed in the feed water were in the range of 1.2-1.5 mg/L.

2.4.1.14. Disinfection By-Product Enumeration

Methodology for DBP enumeration is adapted from (34). Chlorination by products were enumerated under the following conditions:

pH: 8 ± 0.20

Temperature: 23 ± 1ºC

Incubation Time: 24 ± 1 h

Residual chlorine: ~ 2mg/L and > 10mg/L

A preliminary study was undertaken where a 24 hour chlorine demand test was conducted before dosing the samples. In these tests, a variety of dosing conditions were employed for feed water as well as permeate water so as to get the chlorine demand of the respective samples. Two chlorine residuals one high (~ 10 mg/L) and one low (~ 1 mg/L) were targeted.

Incubation bottles (amber colored with PTFE–faced caps) were soaked in detergent overnight. They were rinsed four times with hot tap water and three times with deionized (DI) water and then immersed in chlorine solution (10-20 mg/L, made with DI water) for at least 24 h. After soaking in chlorine solution, glassware were rinsed four times with DI water and then three times with nanopure water; dried in oven at 140 ºC for a minimum of 12 hours. Dosing pipettes were stored in ~ 50 mg/L Cl_2 (made with laboratory clean water). Rinsing with dosing solution was performed three times before use. These precautions were taken to ensure that all glassware employed during DBP enumeration were chlorine demand free.

Before chlorine dosing, water samples were buffered to pH 8 with 2.0 mL/L borate buffer: pH 8 buffer solution was made using 1.0 M boric acid (ACS grade) and 0.26 M sodium hydroxide (ACS grade) in boiled nanopure water.

A combined hypochlorite/buffer solution was made by buffering the hypochlorite solution to pH 8.0 with 6.7 borate buffer. pH 6.7 borate buffer was added to chlorine solution (1,000-4,000 mg Cl_2 /L) to yield a pH 8.0 dosing solution. A 4-5:1 volume ratio of pH 11.2 hypochlorite solution to pH 6.7 borate buffer has been found to yield a pH 8.0 combined hypochlorite/buffer solution, with an approximately 20% drop in chlorine strength (34). Preparing dosing solution (combined OCl^-) allowed us to limit the dosing volume to < 1% of the water sample volume (*e.g.* 5.0 mL dosing solution in 1 L bottle).

pH 6.7 borate buffer solution was prepared by 1.0 M boric acid (ACS grade) and 0.11 M sodium hydroxide (ACS grade) in boiled nanopure water. The dosing procedure consisted of the following steps:

Add 2.0 mL/L pH 8.0 buffer to water sample

1. Adjust to pH 8.0 with H_2SO_4/NaOH
2. Fill incubation bottle ¾th full with buffered water sample
3. Dose with combined hypochlorite/buffer solution holding pipette just above water surface.
4. Cap bottle, invert twice
5. Fill to top with buffered water sample and cap headspace free
6. Invert 10 times
7. Incubate in dark at 20 °C for 24 h
8. After incubation period, measure chlorine residual, pH, and sample for DBPs.

Haloacetic Acids*:* Nine HAAs (monochloro-, dichloro-, trichloro-, monobromo-, dibromo-, bromochloro-, bromodichloro-, dibromochloro-, and tribromoacetic acid) were analyzed by liquid/liquid extraction followed by derivatization with acidic methanol and by gas chromatography with electron capture detector according to USEPA Method 552.2 (35). All DBP calibration standards and internal standards were purchased from Supelco Inc. (Bellefonte, PA). In accordance with EPA method 552.2, calibration curves were generated with 5 points. Calibration standards ranged between 1-100 µg/L. Fresh 100 µg/L standard solution was made before analysis from a 2000 mg/L primary stock solution. A typical monochloroacetic acid calibration curve is shown in Figure 2.6.

The summary of the HAA analysis method is as follows: 40 mL of each sample to be analyzed was spiked with 20 µL of the 10 mg/L 2- Bromopionic acid surrogate solution using 25 µL syringe. Sample pH is adjusted to < 0.5 using concentrated sulfuric acid (4 mL of concentrated sulfuric acid was found to be adequate with all sample matrices in this study). After the solution had cooled, 4 mL of MTBE was

added to each of the samples. Then samples were placed in shaker for 30 minutes. After this step, approximately 2 mL of the upper MTBE layer was transferred to 50 mL bottle. The HAAs that have been partitioned into the organic phase were then converted to their methyl esters by the addition of acidic methanol. Finally, the well-capped bottles were placed in the heating block at 50 ºC for 2 h to achieve meythylation. The acidic extract was neutralized by a back-extraction with a saturated solution of sodium bicarbonate. 0.5 mL of the upper MTBE layer was transferred to an autosampler vial and the target analytes were identified and measured by capillary column gas chromatography using an electron capture detector. Analytes were quantified using procedural standard calibration. Some important details of the column and instrument operation are given next.

GC column: DB-5.625 fused silica capillary with chemically bonded (5% phenyl)-methylpolysiloxane), fused silica column, 30m x 0.25mm ID, 0.25 μm film thickness. Injector temperature = 200 ºC, detector temperature = 280 ºC, Helium linear velocity = 24 cm/s at 35 ºC, splitless injection with 30 second delay. Program: Hold at 35 ºC for 20 minutes, ramp to 75 ºC at 5 ºC per minute and hold for 9.5 minutes, ramp to 225 ºC at 20 ºC per minute and hold for 10 minutes.

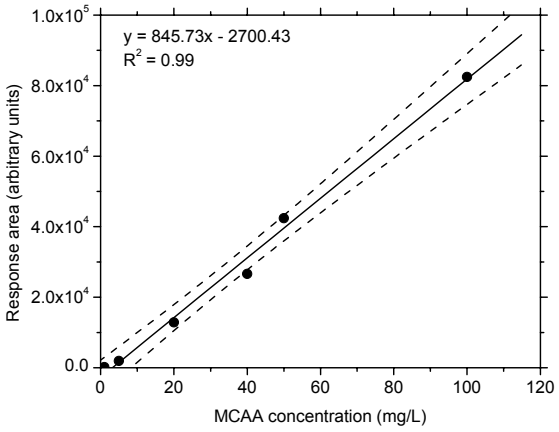

Figure 2.6. A typical calibration curve for MCAA measurement using gas chromatography. The solid line denotes the best fit where as the dashed lines represent the 95% confidence intervals of the mean of the observations.

THMs, Other DBPs, and Chlorinated Solvents*:* Eighteen neutral extractable DBPs were analyzed by liquid/liquid extraction with tertiary-butyl methyl ether and by gas chromatography with electron-capture detection according to U.S. Environmental Protection Agency (USEPA) Method 551.1 (36). These DBPs consisted of four THMs (chloroform, bromodichloromethane, dibromochloromethane, and bromoform); four halacitonitriles or HANs (trichloro-, dichloro-, bromochloro-, and dibromoacetonitrile); two haloketones (1,1, di- and 1,1,1-trichloropropane), chloral hydrate, chloropicrin and five other chlorinated solvents (carbon tetrachloride, 1,2-dibromo-3-chloropropane, 1,2-dibromomethane tetrachloroethylene, 1,1,1,-trichloroethane, and trichloroethylene.

Summary of the method employed is as follows: 50 μL of surrogate analyte solution was added to each of the 40 mL samples to be analyzed in clean 50 mL vial. Following this step, 4 mL of MTBE was added to each of the samples. Then samples were placed in shaker for 30 minutes. After this step exactly 1 mL of the upper MTBE layer was transferred to an auto sampler vial where 10 μL of internal standard primary dilution standard solution was added. Extra care was taken to make sure that no water has carried over onto the bottom of the auto sampler vial. Target analytes were identified by comparing retention times to retention data from the calibration standard analysis and measured by capillary column gas chromatography using an electron capture detector (GC/ECD). Analytes were quantified using procedural standard calibration. Typical calibration curve for BDCM is shown in Figure 2.7. Selected important details of column employed along with instrument operation are given next.

GC column: DB 1701 fused silica capillary with chemically bonded (14% cyanopropylphenyl)-methylpolysiloxane)], 30m x 0.25mm ID, 0.25 μm film thickness. Injector temperature = 200 ºC, detector temperature = 280 ºC, Helium linear velocity = 25 cm/s at 35 ºC, splitless injection with 30 second delay. Program: Hold at 30 ºC for 20 minutes, ramp to 50 ºC at 2 ºC per minute and, ramp to 225 ºC at 10 ºC per minute and hold for 15 minutes, and ramp to 260 ºC at 10 ºC and hold for 30 ºC.

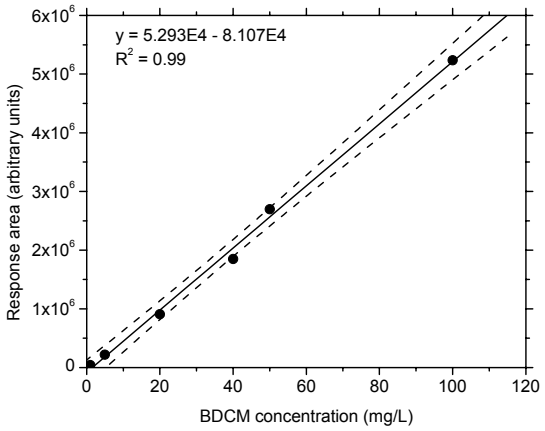

Figure 2.7. A typical calibration curve for BDCM analysis using gas chromatography. The solid line denotes the best fit where as the dashed lines represent the 95% confidence intervals of the mean of the observations.

2.4.3. Natural Source Water

Natural waters were obtained following two pretreatment methods to study their effects on nanofiltration fouling:

- Coagulation (using alum) and filtration using a commercial membrane (Zenon Enhanced Coagulation ZeeWeed-1000 UF package system, Zenon Environmental Corporation, Burlington, ON, Canada). These samples were obtained from the pilot facility at the City of Houston's East Water Purification Plant on two separate occasions and are designated as Sample A and Sample C in this report.
- Coagulation (using alum) and sedimentation at full-scale plant and is designated as Sample B in this report.

Samples A and C were directly fed to the NF membrane without any further treatment. Sample B was additionally treated using a cartridge filter nominally rated at 5 μm (Ryan Herco, Houston, TX), prior to nanofiltration. This was employed to simulate granular media filtration as would be employed at full-scale. Feed water characteristics along with the sampling dates are presented in Table 2.1. The DOC concentrations of the NF feed waters can be classified as being in the medium range (4.5-5 mg/L) and the bromide ion concentration (40-50 μg/L) can be classified as being low.

2.4.4. Synthetic Feed Water

Synthetic feed waters were also employed to better study fundamental transport characteristics of model organics across NF membranes. Polyethylene glycols (PEGs) of various molecular weights were selected because a) they are highly water-soluble, b) can be readily obtained with narrow molecular weight distributions, c) their intrinsic physical properties of relevance to transport modeling can be easily obtained from the literature or can be theoretically calculated and d) they are neutral compounds thereby reducing confounding effects of charge and solution chemistry in their transport across NF membranes.

All experiments were conducted using reagent grade PEGs (MW- 3,500, 7,500, 10,000, 20,000, 35,000 and 100,000 Da), corresponding to 8 mg/L of DOC and 1mM NaCl as a background electrolyte in

nanopure water. PEGs ranging from 3,500 to 10,000 Da and 20,000 to 100,000 Da were obtained from Polyscience (Warrignton, PA) and Fluka Chemical Co. (Milwaukee, WI), respectively. Two suppliers were selected so as to obtain the narrowest molecular weight distributions available commercially.

During each experiment, feed water DOC and conductivity were monitored at least 5 times. Multiple measurements of DOC and feed water conductivity revealed that feed water composition remained same over the entire duration of the experiment. This implied that the contents of the feed tank were well mixed.

2.4.5. Bench Scale Nanofiltration Apparatus

Crossflow experiments were conducted at constant flux without recycling any portion of the concentrate stream, using a pressurized cell (Sepa CF cell, Osmonics, Minnetonka, MN) that accommodates a 19 cm $\times$ 14 cm of a flat membrane sheet (effective filtration area 155 cm^2). The membrane was sandwiched between the two stainless steel plates and placed in a anodized aluminum cell holder. Compressed air was applied to the top of the cell holder, causing a piston to extend downward and compress the cell body against the cell holder base. Double O-rings in the cell body provided a leak proof seal. In order to maintain a leak proof system, the pressure applied on the piston was always greater than transmembrane pressure. The maximum pressure used on the piston was around 200 psi. Feed and permeate spacers were employed to simulate hydrodynamics of spiral wound modules. Two pressure gauges and a flow meter in conjunction with pressure sensors and a flow sensor were employed to monitor important process parameters. Flow meter (P-32046-16, Cole-Parmer instrument company, Chicago, IL) with high accuracy control valve (16 turns) was employed on the waste stream so as to control the recovery accurately. A schematic of the bench scale apparatus is shown in Figure 2.8. Following paragraphs describe the various electronic components used in the bench scale setup.

Continuous near pulse free flow of the feed water was achieved using a Micropump head (74011-11,Cole Parmer instrument company, Chicago, IL) fitted on a console drive (752525-00, Cole Parmer instrument company, Chicago, IL). This enabled a maximum differential pressure of 125 psi and a system pressure of 500 psi. Wetted parts in the pump head included a 316SS body, Ryton® gears, and bearings to reduce the potential frictional losses on the gears.

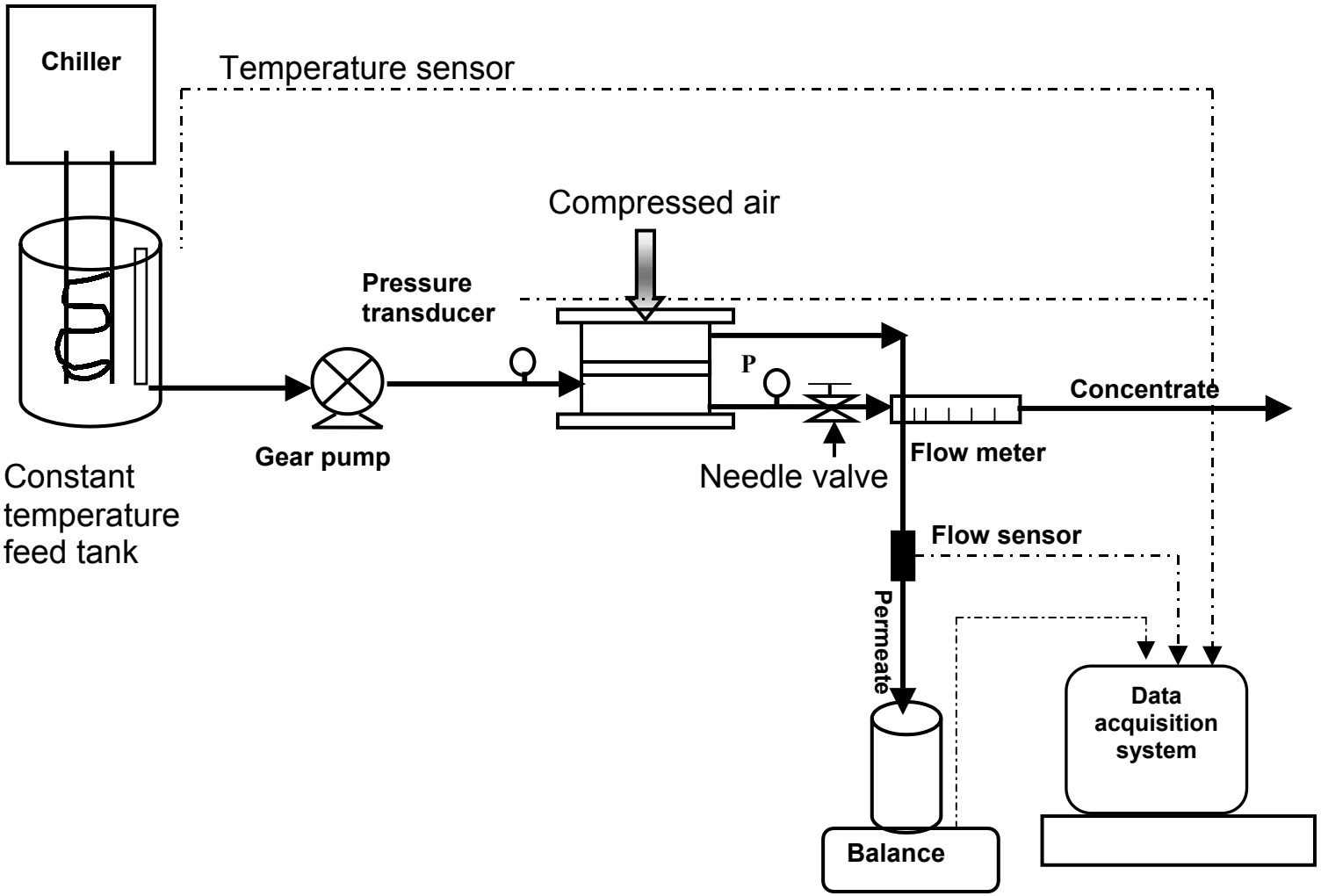

Figure 2.8. Schematic of the bench scale nanofiltration apparatus.

Table 2.1. Summary of source water characteristics

Designation	Date of Sampling	DOC conc. (mg/L)	UV_{254} (cm^{-1})	Br^- conc. (mg/L)	Ca^{2+}(mg/L)	pH	Conductivity (μS/cm)	Alkalinity conc. (mg/L as $CaCO_3$)	TTHM precursor conc. (μg/L)	HAA9 precursor conc. (μg/L)
A	01/16/01	4.50	0.100	46.8	52	7.85	373	64	149.6	173.2
B	01/16/01	5.30	0.100	43.8	48.6	7.77	375	63	121.7	139.1
C	01/26/01	5.06	0.115	39	n/a	7.83	309	not measured	180.5	184.7

2.4.6. Clean Membrane Resistance

Clean membrane resistance was calculated using a variety of flux and pressure pairs for a given membrane coupon using 1 mM NaCl solution. The pressure range was selected in such a way to bracket all the possible operating pressures (20-70 psi). Clean membrane resistance and salt rejection values were used to evaluate the differences in the coupons employed from the same sheet of membrane.

2.4.7. Solute Mass Balance

Conductivity, DOC, and UV_{254} were measured on permeate, concentrate and feed waters. Thus, mass balance closure errors were calculated on each of these parameters to assess the accuracy of sampling protocol, water quality analyses, and flow measurements. The mass balance closure error was calculated in two steps. First the concentrate concentration is calculated from Equation (6). Next, the fractional mass balance closure error was determined by comparing the calculated reject concentration ($C_{c(calc)}$) with the measured reject concentration $C_{c(meas)}$ as follows:

$$Error_{MB} = \frac{(C_{c(meas)} - C_{c(calc)}) \times 100}{C_{c(meas)}} \tag{15}$$

2.4.8. Nanofiltration Experiments

Prior to conducting experiments with synthetic water or natural water, a new membrane was soaked in 1 mM NaCl solution that was replenished 3-4 times over a 24 hour period. Next 1 mM NaCl solution was passed through the experimental set-up for 24 h. During this period, steady clean water flux as well as conductivity rejection was achieved. Following this clean membrane setting, constant flux experiments were conducted at variety of recoveries namely, 5%, 15%, 30%, 40%, 50%, 77%, and 90%, respectively in random order. Operating flux selected in this study ranged from 4 to 25 $L/m^2.h$. During this study constant flux experiments were conducted continuously with each membrane for a period of ~ 100 h at variety of recoveries. Experiments at various recoveries were conducted in succession without any membrane cleaning. During this time, conductivity, or UV_{254} of feed, permeate and reject waters were measured to ascertain steady state (defined in this study as < 4% change in the permeate water collected over the span of 1h, and < 5% change in allowable mass balance closure error). For natural water experiments, once the steady state were ascertained, 1.5 L of permeate water was collected to conduct all required water quality analyses.

2.4.9. Data Acquisition System

LabVIEW (version 5.1, National Instruments, Austin, TX) was the software used for instrument control and data acquisition using a personal computer. It is a graphical programming language that uses icons to create applications for remote digital control of various types of instruments. It makes use of Data Flow programming, where the flow of data determines execution. A user interface (front panel) was built by using a set of tools and objects. Code was added using graphical representations of functions to control the front panel objects. The user interface developed in this study is depicted as a block diagram in Figure 2.9. Two analog channels were utilized in the input mode to acquire signals from the pressure transducer and the temperature probe. All connectors marked ground or negative were connected to the AIGND pin of the corresponding channel and all the connectors marked positive were connected to the corresponding channel pins. The weighing balance was connected directly to the RS232 serial port and the readings were taken every minute. Finally, all measurements were saved in Microsoft Excel format.

A flow chart depicting the logic employed and program execution is shown in Figure 2.10. The algorithm used for data acquisition is explained next:

1) Start the program
2) Initialize the Time Count to zero so that the time utilized in each cycle can be recorded correctly.

3) Set Timer to zero

4) Wait for 1 minute

5) Get the pressure of the influent from the pressure transducer, the permeate weight from the weighing balance and the temperature of the feed water from the temperature probe

6) Index this set of readings

7) Check if the user has stopped the program. If not repeat step 3 to step 6. If stopped go to step 8

8) Form a 2-Dimensional array of time, pressure, weight and temperature

9) Write it to an Excel spread-sheet

10) Stop

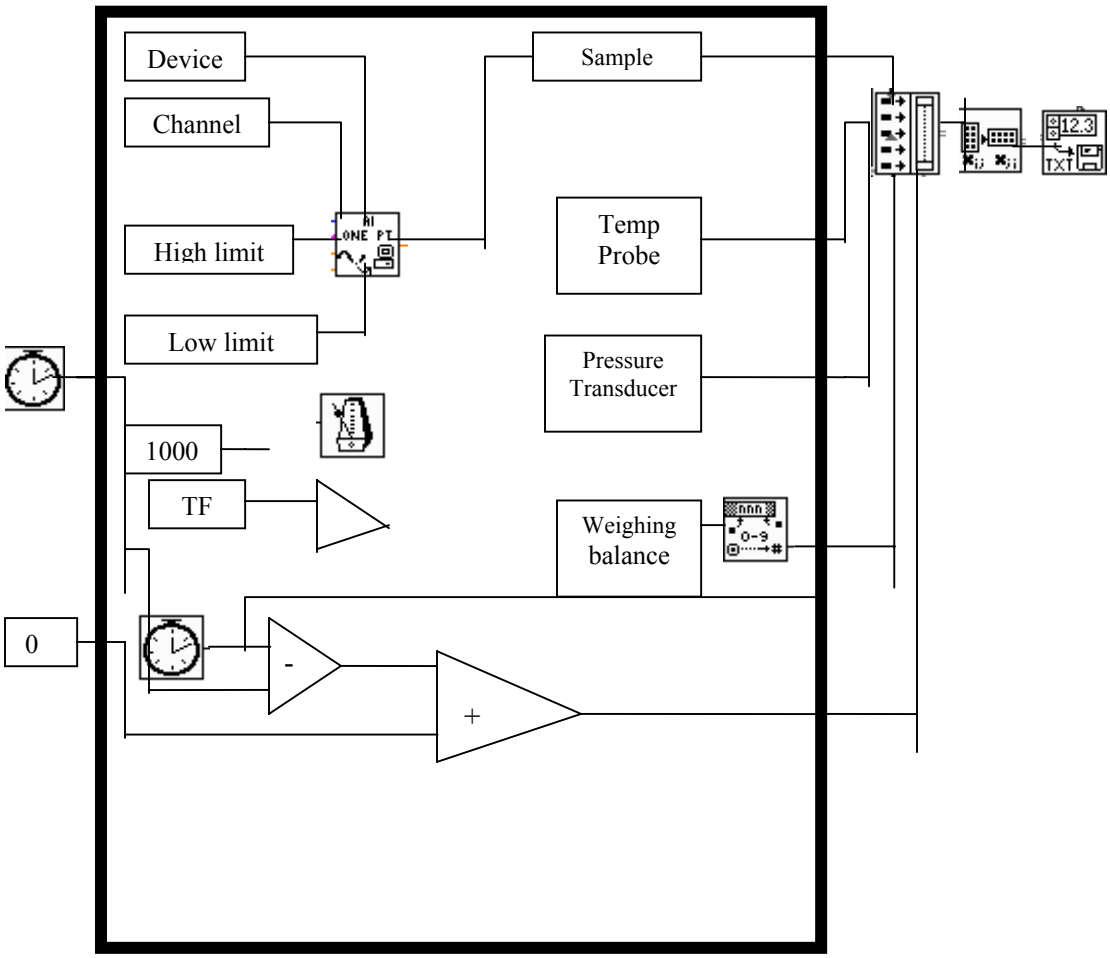

Figure 2.9. Block diagram of the data flow used in the Data Acquisition System.

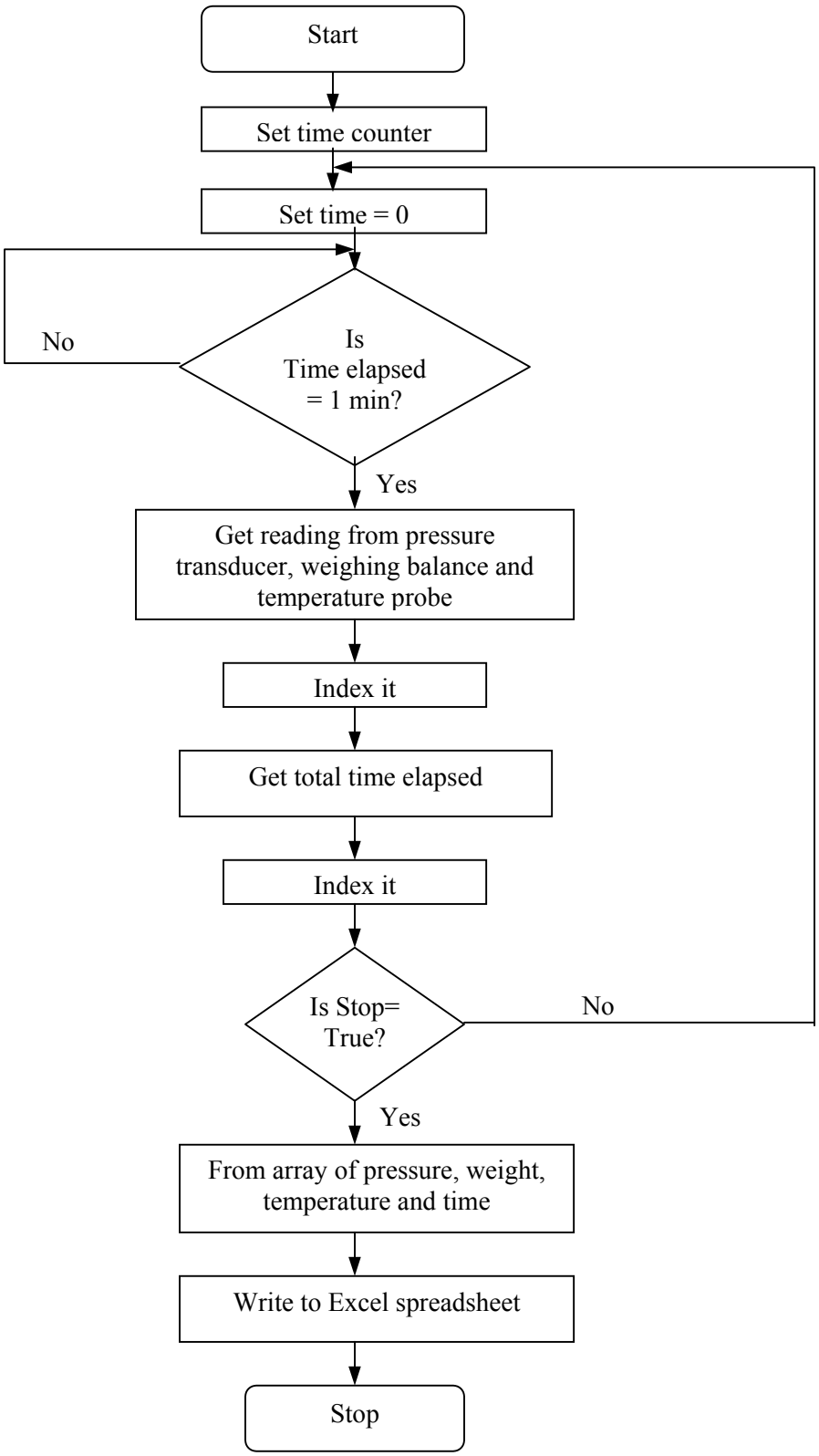

Figure 2.10. Flowchart of the logic employed for computerized data acquisition.

A Peripheral Component Interconnect card (PCI 6024E, National Instruments, Austin, TX) was installed for online data acquisition using LabVIEW software. A PCI is an I/O bus i.e. it is a channel over which information flows between the computer and the various devices connected to its peripherals. It can obtain approximately 200 kilo-samples per second and has a 12- bit performance on 16 single ended analog input. It can accommodate two 12-bit analog outputs, eight digital I/O lines and two 24-bit counters.

A 68-pin connector block (National Instruments, Austin, TX, Model No. CB-68LP) was used as a connection board to externally wire the output of instruments to the particular channel of the PCI card. A ribbon cable (National Instruments, Austin, TX, Model No. R6868-68) was used to connect the connector block to the PCI card installed in the computer.

2.4.10. Pressure Transducer

Two 0.5 – 5.5V pressure transducers were employed for continuous pressure monitoring (PX303-050G5V and PX303-100G5V, Omega Engineering Company, Stamford, CT). The PX303-050V model has a full scale range of 0 – 50 psi and the PX303-100G5V has a range of 0 – 100 psi. Both pressure transducers were excited using 24VDC from an external power supply. The pressure transducer responded with a minimum time of 1 ms. Thus readings were taken only after a gap of 1 minute to minimize electronic error in pressure measurement. Both these transducers were calibrated prior to use. The 50 psi transducer was calibrated using a glycerin filled pressure gauge of 0 – 100psi range (U-68022-04, Cole Parmer, Vernon Hills, Illinois) whereas the 100 psi pressure transducer was calibrated using a glycerin filled pressure gauge of 0 – 200psi range (U-68022-03, Cole Parmer, Vernon Hills, Illinois). Both these gauges have an accuracy of ±1%. The calibration curves for the 50 psi and 100 psi transducers are depicted in Figures 2.11 and Figures 2.12 respectively.

A power supply (U24Y101 24VDC, Omega Engineering Company, Stamford, CT) was used to provide the required excitation voltage to the pressure transducers. It has a built-in fuse of 0.5amps, 250V to prevent damage due to short circuits or prolonged overloading.

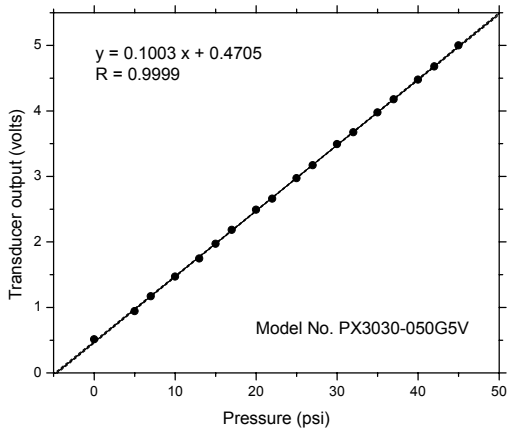

Figure 2.11. Calibration curve for the 50 psi pressure transducer. The solid line denotes the best fit and the dashed lines represent the 95% confidence intervals of the mean of the observations.

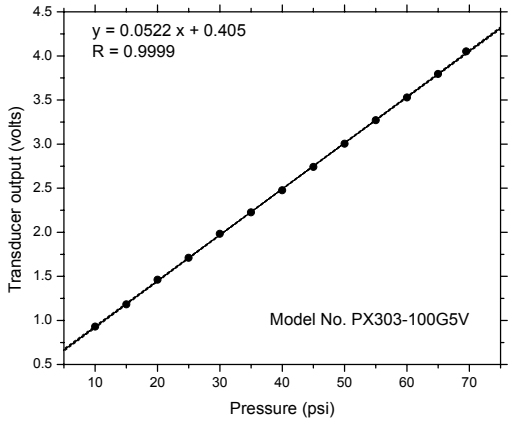

Figure 2.12. Calibration curve for the 100 psi pressure transducer. The solid line denotes the best fit and the dashed lines represent the 95% confidence intervals of the mean of the observations.

2.4.11. Weighing Balance

The permeate water was continuously collected on a weighing balance (Ohaus Navigator N1H110, Fisher Scientific, Houston, TX). The balance had a full scale range of 0-8100 g, a least count of 0.5 g, and also displayed the weight on its LCD panel. The in-built RS232 port in the balance was directly connected to

the computer to obtain digital signal corresponding to the weight. The LabVIEW program recorded the reading displayed on the balance every one minute. Since the stabilization time for this balance is 3 seconds, there was no error.

2.4.12. Temperature Probe

The temperature of the feed tank was recorded using a 12 inch, rugged temperature probe (TJ120 CPSS 116G, Omega Engineering Company, Stamford, CT). A grounded probe was used as it reduces the response time to 0.04 sec. The probe had a temperature range of 0-200 °C and an output voltage range of 0-10V. A signal conditioner (CCT-24-0/200C Omega Engineering Company, Stamford, CT) was employed to convert the signal from a T type thermocouple to a conditioned isolated analog output. The Temperature probe calibration curve is given in Figure 2.13.

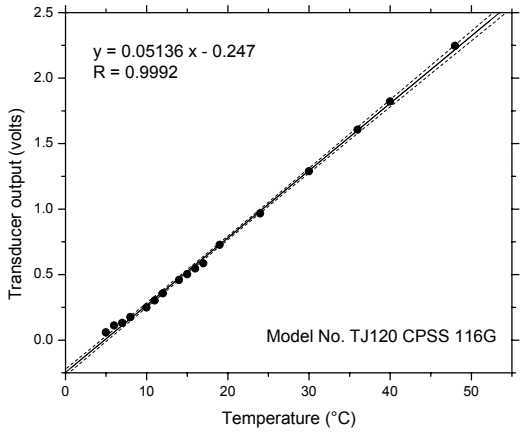

Figure 2.13. A typical calibration curve for the temperature probe. The solid line denotes the best fit whereas the dashed lines represent the 95% confidence intervals of the mean of the observations.

2.5. Membrane Fouling Analysis

In this study, selected experiments were conducted to evaluate the effect of pretreatment on NF fouling at constant recovery. Both conventional treatment and microfiltration were investigated as nanofiltration pretreatment processes. Specific flux profiles for membrane TFC-S followed a straight-line decrease with increase in volume of water filtered. Thus, straight-line fits were obtained for normalized specific flux using linear regression techniques.

$$\frac{J_s}{J_{s0}} = -bV + A \qquad (16)$$

Where, J_s (liters per meter squared per hour per bar) = instantaneous specific flux; J_{s0} (liters per meter squared per hour per bar) = initial specific flux; V = cumulative volume of water filtered (L). The parameters A and b (L^{-1}) were statistical best fit values of the initial normalized specific flux and the fouling rate, respectively. A, b and the corresponding confidence intervals were calculated using linear regression method. Equation 16 relates normalized specific flux and the corresponding volume filtered. Fouling rates in pilot studies typically are determined using time as independent variable, which is useful in deciding the chemical cleaning intervals. However, this approach does not take in to account for the changes in the amount of water filtered. Foulant transport, which is responsible for specific flux decline in membranes, is highly dependent on the volume filtered. Employing Equation 16 is a better method of comparing fouling rates obtained at different fluxes as opposed to using time as the independent variable (37).

3. RESULTS AND DISCUSSIONS

3.1. Solute Mass Balances

Mass balances were conducted around the NF system for DOC and conductivity assuming steady-state condition (no accumulation in the membrane module). Typical comparisons of the experimentally observed and theoretically predicted waste stream concentrations of DOC and conductivity are shown in Figures 3.1 and 3.2 respectively. Two sided, two sample t-tests were performed to statistically compare experimentally measured and theoretically predicted waste concentrations. In all cases there were no differences in the means of the calculated and measured masses in the concentrate water at 0.0225 level of significance (95.50 percent confidence interval). These mass balances show that the sampling protocol was acceptable, and the water quality analyses and flow monitoring was accurate.

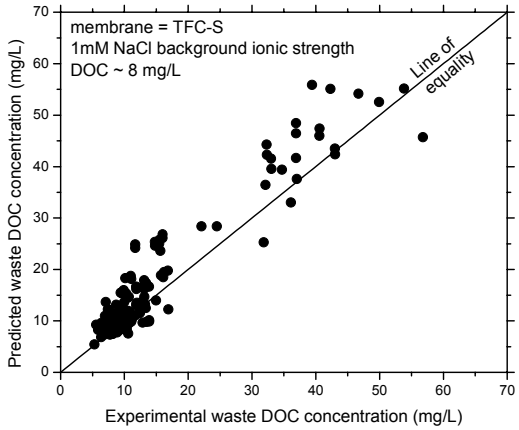

Figure 3.1. DOC mass balance for the concentrate stream.

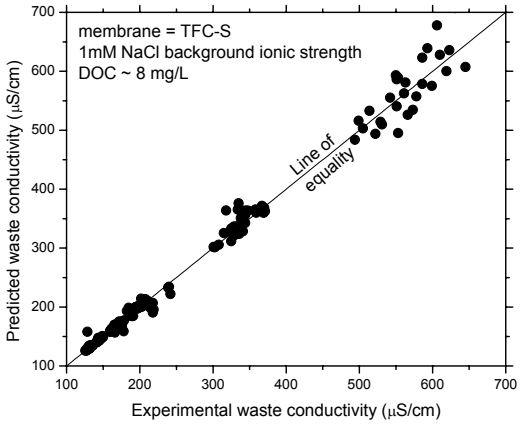

Figure 3.2. Conductivity mass balance for the concentrate stream.

3.2. Clean Membrane Resistance

Figures 3.3 and 3.4 show the clean membrane resistances (R_m) for the TFCS membrane and NTR7450 membrane, respectively. In both cases, the transmembrane flux was found to increase linearly with pressure indicating that membrane compaction effects were negligible in the pressure range employed. The R_m values were the in the range of $3.38 \times 10^{13} \pm 0.30 \times 10^{12}$ m^{-1} and $4.49 \times 10^{13} \pm 1.40 \times 10^{12}$ m^{-1} for the TFCS and NTR7450 membranes respectively. Figures 3.3 and 3.4 also display the 95% confidence interval for the mean R_m (inner dashed lines) and 95% confidence interval for individual observations of R_m (outer dashed lines). These figures were used as quality assurance tool and if the measured R_m values for any given membrane coupon prior to conducting experiments with the test water did not fit in the 95% prediction interval it was immediately discarded and a new one employed for the experiments.

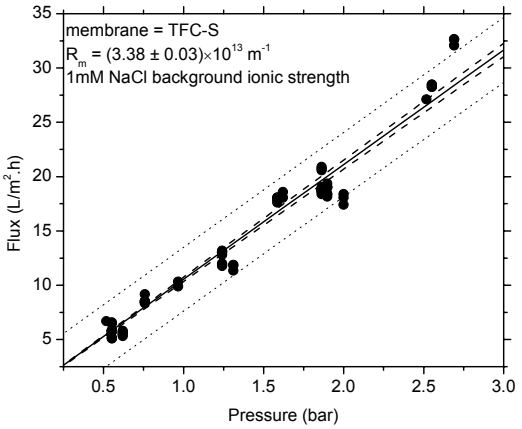

Figure 3.3. Resistances of new TFC-S membranes. Inner dashed lines denotes 95% confidence interval of mean of observations; outer dotted lines denote 95% confidence interval of individual observations.

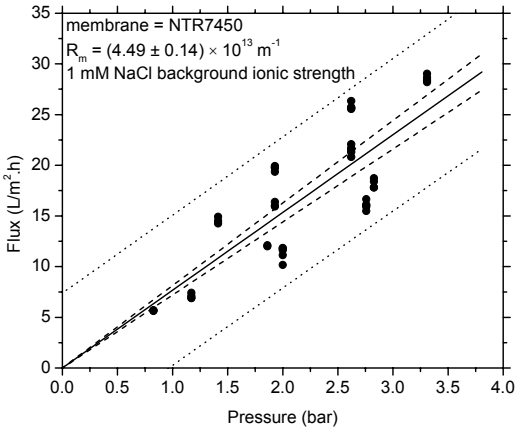

Figure 3.4. Resistances of new NTR-7450 membranes. Inner dashed lines denotes 95% confidence interval of mean of observations; outer dotted lines denote 95% confidence interval of individual observations.

3.3. Typical Flux and Pressure Profiles

Constant flux experiments were conducted by manually adjusting the transmembrane pressure. Typical flux profile and pressure profile are shown in Figures 3.5 and 3.6, respectively. In all experiments, the initial pressure required to achieve the target flux was low but quickly the pressure requirement per unit time increased, followed by low increments of pressure to maintain the desired flux through out the experiment. In the time span between 750 to 1,250 minutes and 2,000 to 2,500 minutes, gradual decease in flux is observed because these correspond to overnight time spans when monitoring was not possible. The pressure required to maintain the constant flux were highly dependent upon recovery. At lower recoveries the transmembrane pressure requirement was lower than the requirements at higher recoveries. The mean steady state flux in Figure 3.5 was 3.67 ± 0.19 L/m^2.h (95% confidence interval) corresponding to a target flux of 4 L/m^2.h.

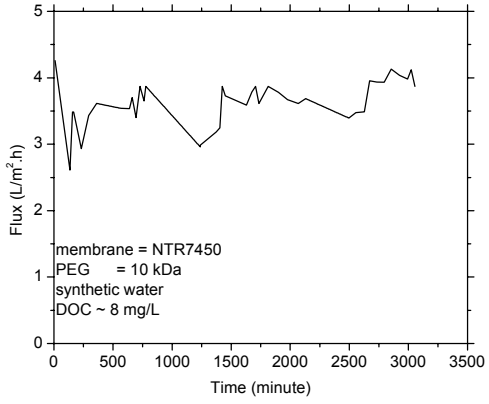

Figure 3.5. Typical constant flux profile for the synthetic and natural water experiments.

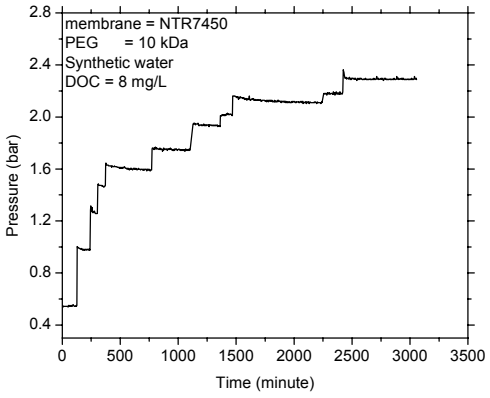

Figure 3.6. Typical pressure profile for the synthetic and natural water experiments.

3.4. Specific Flux Profiles

Typical specific flux profiles for the duration of the experiments using the NTR 7450 membrane is shown in Figure 3.7. It was observed that all membranes experienced an initial rapid specific flux decline followed by gradual decline, indicating that membrane required time to achieve stable performance with respect to the test water as a result of concentration polarization, gel layer formations, and adsorbed organic layers. Overall, the NTR7450 and TFC-S membranes experienced relatively stable operation throughout the duration of the experiment. The analysis of membrane fouling has been discussed in more detail in sections 2.5 and 3.6.

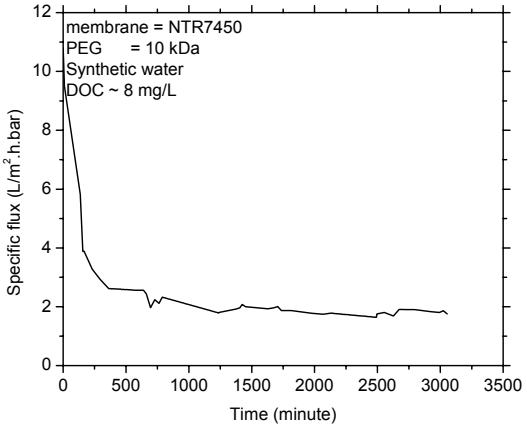

Figure 3.7. Typical specific flux profile for NTR7450 membrane.

3.5. Temperature Profile

Permeate flux and solute rejection is expected to be a strong function of water temperature. Therefore, experiments were conducted in controlled temperature environment to minimize the effects of temperature variation. Typical temperature profile is shown in Figure 3.8. The mean temperature was observed to be around 23.48 ± 0.04 °C (error bar represents 95 percent confidence interval limit). The low magnitude of error bar indicates that constant temperature was maintained during the entire experimental run.

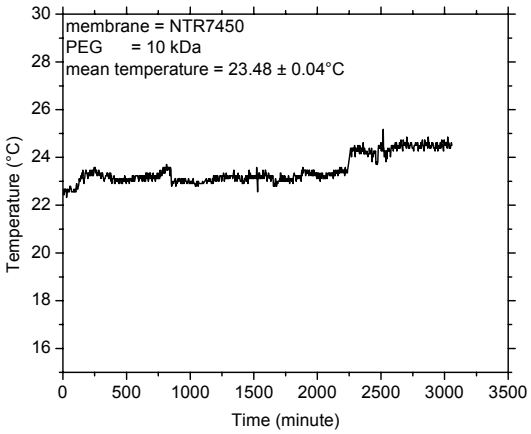

Figure 3.8. Typical constant temperature profile for the synthetic and natural water experiments.

3.6. Membrane Fouling

Fouling rate parameters obtained from Equation 16 for the experiments conducted at 77% recovery are summarized in Table 3.1. The error bars represent 95 percent confidence intervals of the best-fit straight line obtained using linear regression. The initial fouling rate was observed to be higher for conventionally treated water than membrane pretreatment. Even after the specific flux stabilized, the fouling rate for conventionally treated water appeared to be higher as compared to water pretreated using membranes. Thus, in the range of experimental conditions investigated, NF fouling rates were decreased somewhat when membrane pretreatment was employed compared with conventional treatment.

However as can be seen in Table 3.1, fits were poor in many cases and the fouling rates were indistinguishable from zero at 95% confidence. Further, these short term experiments were conducted primarily with the intention of studying effects of nanofiltration on permeate water quality. Hence, these results on fouling should be interpreted with caution.

Table 3.1. Summary of statistical fits to relative flux decline for natural water experiments (source A and Source B) at 77% recovery. Error bars indicate 95 percent confidence intervals.

Membrane	Source Water	Flux ($L/m^2.h$)	Fouling rate (L^{-1})	R^2
TFC-S	Source A (membrane pretreatment)	15.65 ±0.64	0.123 ±0.055	0.74
		15.65 ±0.64	-0.006 ±0.023	0.27
		7.84 ±0.10	0.006±0.006	0.33
		19.85 ±0.20	0.008 ±0.004	0.76
	Source B (conventional pretreatment)	14.95 ±1.00	0.353 ±0.004	0.86
		14.95 ±1.00	0.018 ±0.003	0.92
		9.04 ±0.50	-0.023 ±0.012	0.74
		20.28 ±0.39	0.020 ±0.027	0.42
		25.94 ±1.03	-0.018 ±0.015	0.60

3.7. Permeation of Polyethylene Glycols, Natural Organics, and DBP Precursors

Water quality data from drinking water treatment NF studies are often presented either as rejection or merely as permeate concentrations (4-6, 8, 38). Because the transport of diffusion-limited solutes depends on permeate flux, feed water recovery, and possibly on feed concentrations, a simplistic presentation of just permeate concentrations or rejection does not allow comparison of data obtained from various locations, operating conditions, and/or membrane types. Additionally, it precludes predictions of permeate concentrations if operating conditions were changed. In other words, rejection is only an apparent membrane property. In contrast, employing intrinsic membrane transport parameters facilitates scale-up calculations of permeate water quality, allows projections of permeate concentrations with varying recovery and flux, and represents a more accurate comparison of separation characteristics (39).

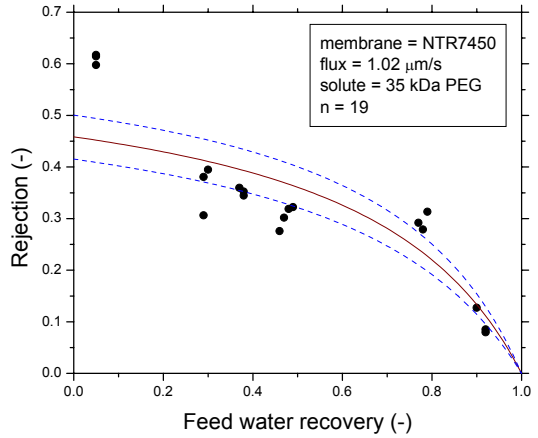

Figure 3.9. Effect of feed water recovery on rejection of PEG (35 kDa) using NTR7450 membrane.

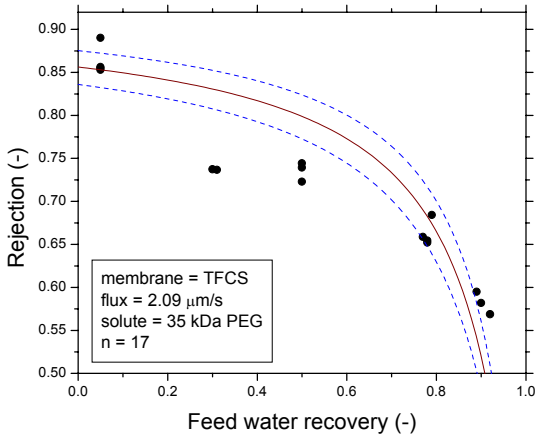

Figure 3.10. Effect of feed water recovery on rejection of PEG (35 kDa) using TFCS membrane.

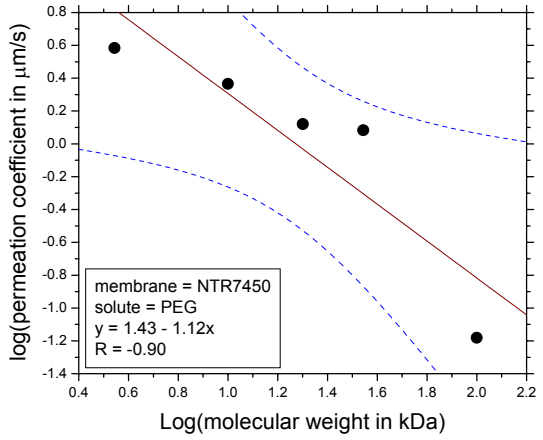

Figure 3.11. Effect of PEG molecular weight on its permeation across NTR7450 membrane.

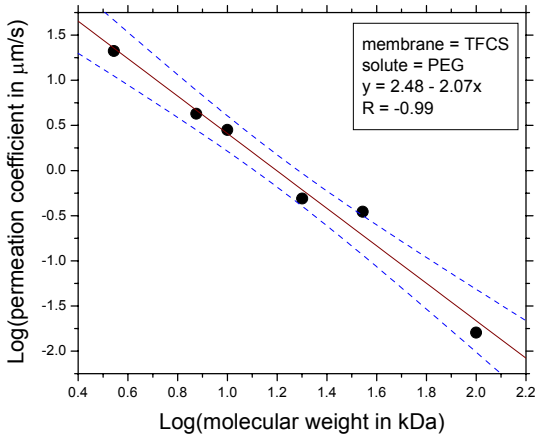

Figure 3.12. Effect of PEG molecular weight on its permeation across TFCS membrane.

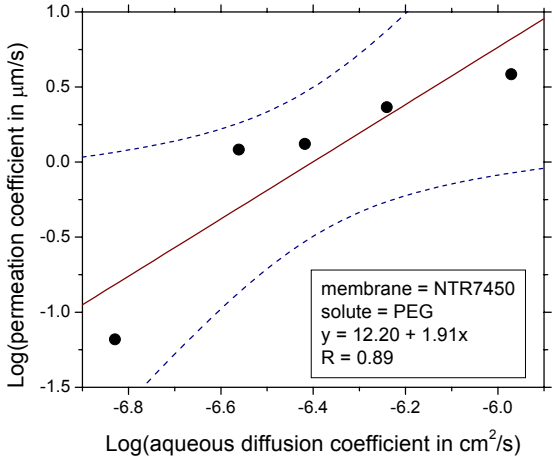

Figure 3.13. Effect of PEG diffusivity on its permeation across NTR7450 membrane.

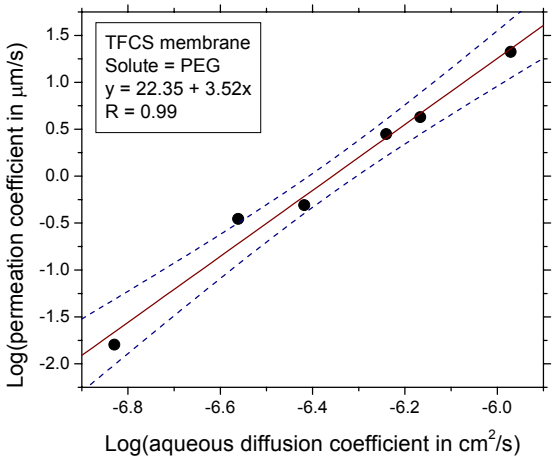

Figure 3.14. Effect of PEG diffusivity on its permeation across TFCS membrane.

Using the technique of profiling, (see section 2.2) we have recently shown that the permeate water quality model given in Equation 10 exhibits severe non-linearity leading to very poor precision of parameter estimates (21). In many instances, upper confidence limits of these parameters estimated data were unbounded. However, eliminating the back-diffusion coefficient (k_b □ □) results in Equation 17 and allows the estimation of upper confidence limits for the solute permeation coefficient. Mechanistically, this is equivalent to ignoring Fickian transport away from the membrane surface caused by concentration polarization. Due to the increased precision of parameter estimates, Equation 17 that employs only a solute permeation coefficient was used predominantly in this study.

$$R = 1 - \frac{k_s}{k_s + \frac{2J_w(1-R_f)}{2-R_e}} \qquad 17$$

The permeation coefficient has been shown to be a very good descriptor of solute transport across thin-film composite NF membranes (21). Increasing k_s values represent higher permeate concentrations (decreasing rejection).

Figures 3.9 and 3.10 depict decreases in polyethylene glycol (35 kDa) with increasing recovery when the flux was maintained at a constant value. A comparison of the scale employed in the y-axis also shows that the TFCS membrane achieved greater removals compared to the NTR7450 membrane. One set of experimental data similar to that depicted in Figures 3.9 and 3.10 was used to calculate one value of the permeation coefficient. Because the TFCS membrane was more retentive to organic contaminants, it was quantified by lower permeation coefficients (k_s values) compared to the NTR7450 membrane. For example, the permeation coefficients for a 20 kDa polyethylene glycol are 1.32 μm/s and 0.49 μm/s for the NTR7450 and TFCS membranes respectively. A complete listing of all permeation coefficients calculated in this study is given in Tables 3.2 and 3.3 for the NTR7450 and TFCS membranes respectively.

Figures 3.11 and 3.12 also depict a straight-line decrease in permeation coefficients of polyethylene glycols as their molecular weight increases (in a log-log scale). This could be caused both by increasing steric hindrance and decreasing diffusivity. Further, as observed in Figures 3.13 and 3.14 log permeation coefficients for both NTR7450 and TFCS membranes increased in a straight-line fashion with increasing log aqueous diffusivity (calculated using the Hayduk and Laudie method as described in section 2.3). Even though these relationships do not offer conclusive evidence of solute transport mechanisms across nanofiltration membranes, they underscore the importance of aqueous diffusion coefficient in determining contaminant rejection.

Table 3.2. Summary of 1 parameter modeling results using the NTR7450 membrane.

Solute	MW (kDa)	k_s (μm/s)	Error (-)	Number of observations
PEG	3.5	3.84	0.159	16
PEG	10	2.32	0.086	15
PEG	20	1.32	0.027	16
PEG	35	1.21	0.106	16
PEG	100	0.07	0.037	14

Precision = 0.0001, tolerance = 0.01, convergence = 0.001.

Table 3.3. Summary of 1 parameter modeling results using the TFC-S membrane.

Solute	MW (kDa)	k_s (μm/s)	Error (-)	Number of observations
PEG	3.5	21.06	0.013	16
PEG	7.5	4.25	0.156	15
PEG	10	2.81	0.245	16
PEG	20	0.49	0.538	15

PEG	35	0.35	0.050	16
PEG	100	0.016	0.014	15
DOC1	NA	1.27	0.012	5
DOC2	NA	1.47	0.062	3
DOC3	NA	1.14	0.023	4
TTHM precursor	NA	0.90	0.018	5
HAA9 precursor	NA	1.62	0.009	5
CH precursor	NA	1.20	0.019	5
CP precursor	NA	2.45	0.049	5
HAN precursor	NA	4.41	0.037	5
HK precursor	NA	3.10	0.050	5
Bromide ion	79.9	2.16	0.114	5
Cl_2 consumption	NA	2.69	0.013	5
UV_{254}	NA	1.68	0.027	5

Precision = 0.0001, tolerance = 0.01, convergence = 0.001.

3.8. Disinfection By-Product Relationships in Nanofilter Permeates

One of the primary reasons for installing municipal drinking water nanofiltration plants is the control of disinfection by-products. Chlorination of drinking waters containing organic carbon results in the formation of potentially carcinogenic, teratogenic and mutagenic by-products, including trihalomethanes (THMs) and haloacetic acids (HAAs). Because stable analytical standards and methods for bromodichloro-acetic acid ($BrCl_2AA$), dibromochloroacetic acid (Br_2ClAA), and tribromoacetic acid (Br_3AA) were only recently developed, most studies have not measured all nine HAAs containing bromine and chlorine. Consequently, only five HAAs: monochloro-, dichloro-, trichloro-, monobromo-, and dibromoacetic acid (ClAA, Cl_2AA, Cl_3AA, BrAA, and Br_2AA, respectively) are currently regulated under the Disinfectants/Disinfection By-Products (D/DBP) Rule (1). A sixth HAA (viz. bromochloroacetic acid, BrClAA) was included in the Information Collection Rule (ICR) (12). Even though the mixed bromochloro HAA species and Br_3AA are not currently regulated, it is crucial to examine their occurrence and treatability in drinking water because of their potential adverse human health effects.

The very limited number of studies that have reported all nine HAAs containing Br and Cl show that the non-regulated HAAs (BrClAA, Br_2ClAA, $BrCl_2AA$, Br_3AA) can comprise a substantial fraction of the total molar concentration of HAAs (7, 40-42). Almost all prior laboratory-scale investigations of HAA9 speciation have been conducted by holding the dissolved organic carbon (DOC) concentration constant in raw water or commercial or extracted humic acids and artificially spiking various amounts of the bromide ion (40-42). In contrast, nanofiltration (NF) that is one of the most promising methods for DBP control inherently alters the Br^-/DOC ratio between feed and permeate waters, thereby changing DBP speciation upon chlorination (7).

The occurrence of, and correlations between various classes of DBPs have been reported predominantly for conventionally treated waters (43-46). Ultraviolet (UV) absorbance at 254 nm (UV_{254}) and one-cm path length and DOC have been reported to be good surrogates for THM and HAA5 formation during conventional treatment (43, 47, 48). However, surrogates for THMs and HAA9 in NF permeate waters have not yet been comprehensively evaluated. If simple surrogates for DBPs in nanofilter permeates are identified, the need for expensive and time-consuming DBP analyses could potentially be limited to regulatory compliance and more frequent monitoring of these surrogates undertaken. This will allow better process control thereby reducing potentially adverse health effects of various DBPs.

Figures 3.15, 3.16, and 3.17 demonstrate that DOC concentrations, UV_{254}, and chlorine consumed are highly correlated with each other even in NF permeate waters. Interestingly, as observed in Figure 3.18, permeate HAA9 concentrations were always greater than permeate TTHM concentrations on a molar

basis. Therefore, if free chlorine is used as the primary disinfectant when bromide ion concentrations are low, HAA concentrations can be higher than THM concentrations. This was probably caused by low bromide ion concentrations. HAA9 concentrations may have increased if lower pH values had been employed during DBP enumeration (49). However, under the current D/DBP rule, HAAs are regulated at lower mass concentrations than THMs. Thus, a more equitable regulation of these undesirable by-products of water chlorination may be warranted for nanofiltered waters, health effects withstanding.

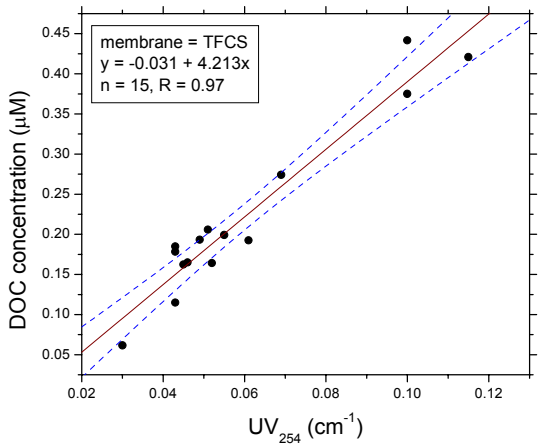

Figure 3.15. Correlation between UV_{254} and DOC concentration.

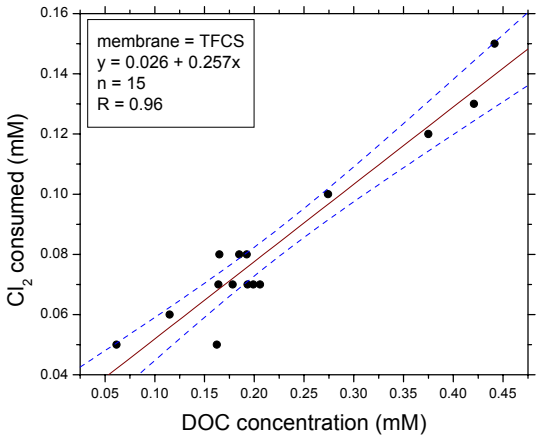

Figure 3.16. Correlation between DOC concentration and Cl_2 consumed.

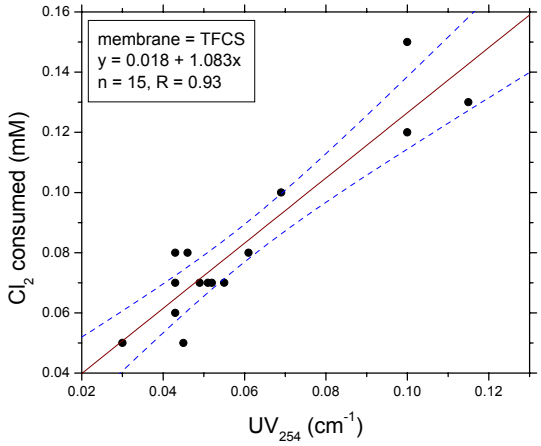

Figure 3.17. Correlation between UV_{254} and Cl_2 consumed.

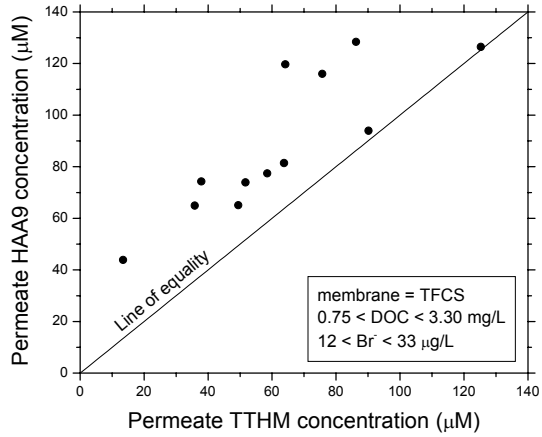

Figure 3.18. Comparison of total THM and HAA9 concentrations in TFCS membrane permeate.

Linear regression analyses were performed to identify possible surrogates for DBPs in permeate waters. Figures 3.19 – 3.24 depict excellent correlations obtained for both TTHMs and HAA9 using DOC, UV_{254} and Cl_2 consumed as independent variables suggesting that they all can be employed as DBP surrogates even in nanofiltered waters. The individual best fit equations, correlation coefficients, and the number of observations are also included in each graph. The dashed lines denote the 95% confidence intervals. Similar results have also been reported for conventionally treated waters (43, 47, 48). These data demonstrate that simpler, more rapid, and cheaper measurements such as UV_{254}, DOC, and Cl_2 consumed can be employed as surrogates for aqueous DBP concentrations even in chlorinated nanofiltered waters.

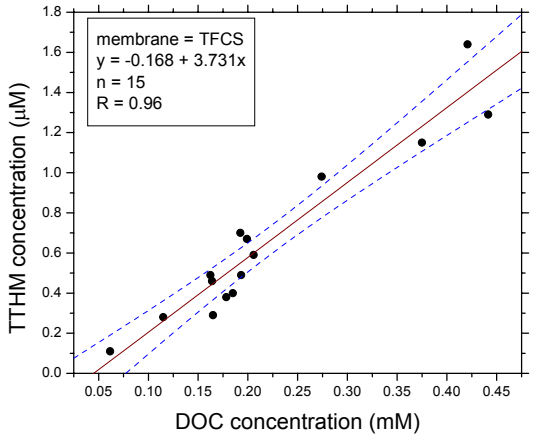

Figure 3.19. Correlation between DOC and TTHM concentration.

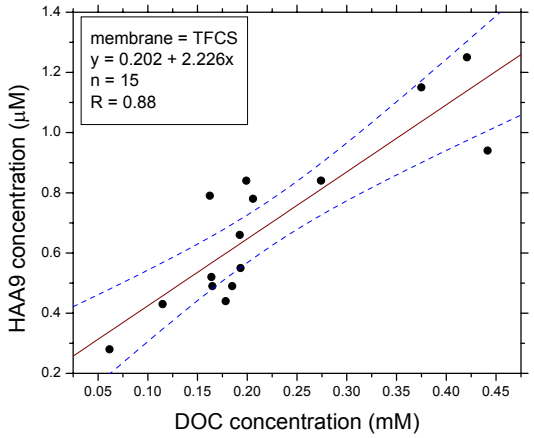

Figure 3.20. Correlation between DOC and HAA9 concentration.

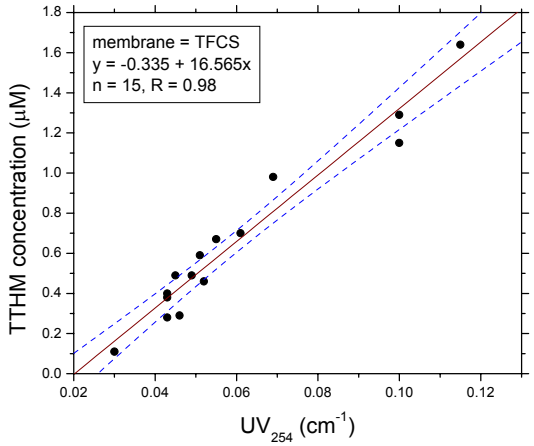

Figure 3.21. Correlation between UV_{254} and TTHM concentration**.**

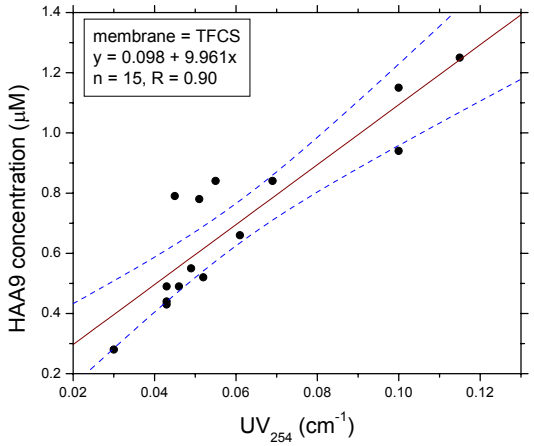

Figure 3.22. Correlation between UV_{254} and HAA9 concentration**.**

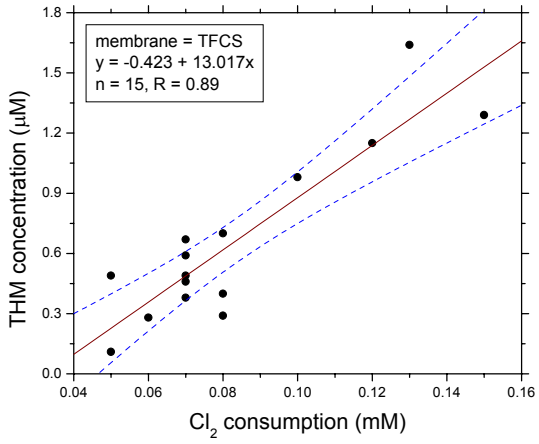

Figure 3.23. Correlation between Cl_2 consumed and total THM concentration.

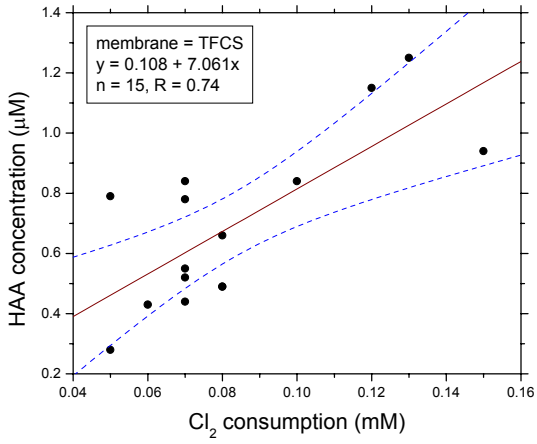

Figure 3.24. Correlation between Cl_2 consumed and HAA9 concentration.

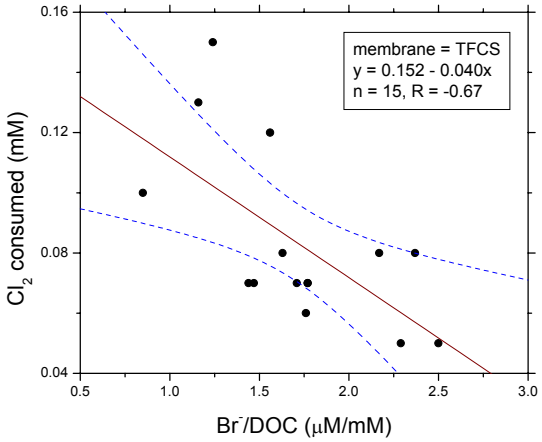

Figure 3.25. Correlation between Br^-/DOC ratio and Cl_2 consumed.

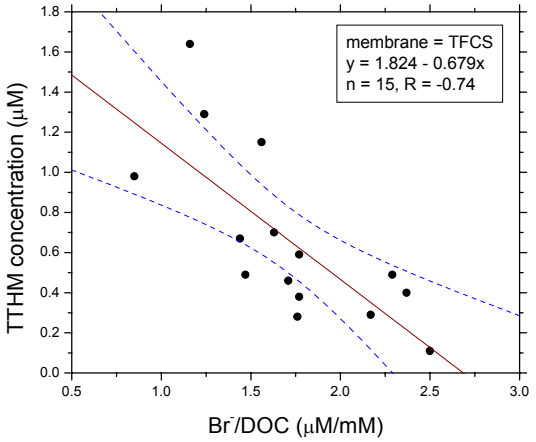

Figure 3.26. Correlation between Br^-/DOC ratio and TTHM concentration.

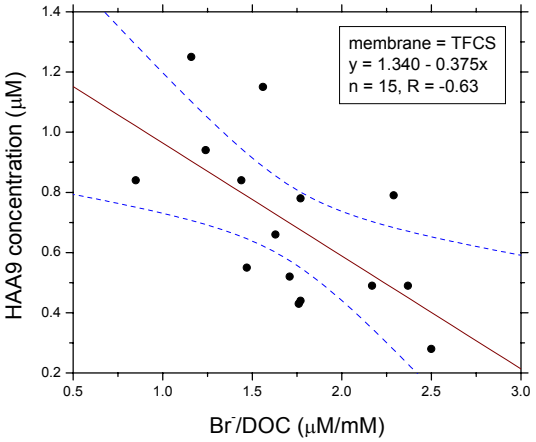

Figure 3.27. Correlation between Br^-/DOC ratio and HAA9 concentration.

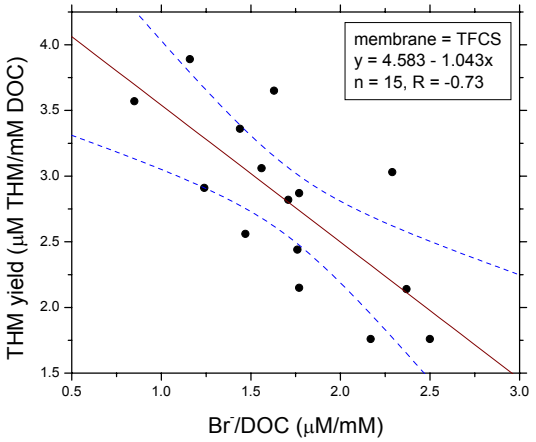

Figure 3.28. Correlation between Br^-/DOC ratio and TTHM yield.

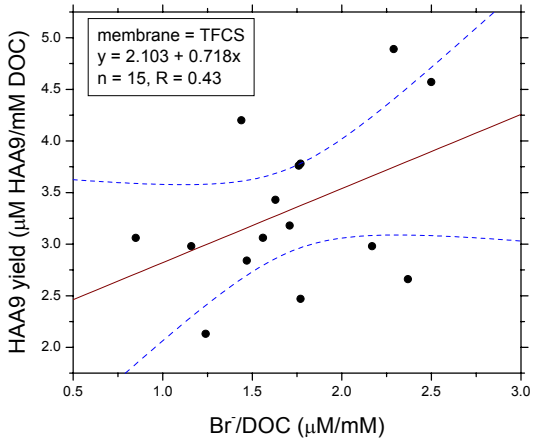

Figure 3.29. Correlation between Br^-/DOC ratio and HAA9 yield.

3.9. Impacts of Changing Br^-/DOC Ratio

Figures 3.25 – 3.29 depict the effects of Br^-/DOC molar ratio on Cl_2 consumed, TTHM and HAA9 concentrations, and THM and HAA9 yield all calculated on a molar basis. As seen in Figures 3.25, 3.26, and 3.27 chlorine consumption, as well as TTHM and HAA9 concentrations decreased in a straight-line fashion with increasing Br/DOC ratio. When Br^- is added to samples with constant DOC levels (increasing the Br^-/DOC), total THM concentrations increase (50-52). Chlorination of humic acid extracts of constant DOC concentrations (0.33 mM), but spiked with various amounts of Br^-, has been reported to yield fairly constant HAA9 concentrations (41). Artificially increasing Br^- concentrations in a high-DOC (0.91 mM) natural groundwater has also been reported to increase HAA9 concentrations following chlorination (42). In contrast to these previous studies, THM and HAA9 concentrations decreased with increasing Br^-/DOC for all permeate waters suggesting that NF permeates were precursor limited.

Figure 3.28 depicts decreasing THM yield (total THM molar concentration normalized by the DOC molar concentration) suggesting that the reactivity of NOM fractions towards THM formation decreased upon nanofiltration. In contrast, Figure 3.29 shows increasing HAA9 yield with Br^-/DOC molar ratio suggesting that nanofiltration may have increased the reactivity of NOM fractions towards HAA9 formation. Another recent study has also reported inconsistent trends in THM and HAA9 yield following nanofiltration (53).

3.10. Disinfection By-Product Speciation

Most NF and DBP studies have been site-specific and have typically reported only reductions in total mass concentrations of specific DBPs (4-6, 8). Even though previous research has demonstrated that NF achieves high removals of DBP precursors (6-8), commonalities in DBP speciation in permeate waters have not been well understood. This may reduce the need for, and extent of site-specific studies. Additionally, it may provide a mechanistic basis for DBP formation leading to improved control strategies as more NF plants are installed. Data on disinfection by-product formation and speciation following nanofiltration of water containing low concentrations of bromide ion (< ~ 0.6 μM) have not yet been reported.

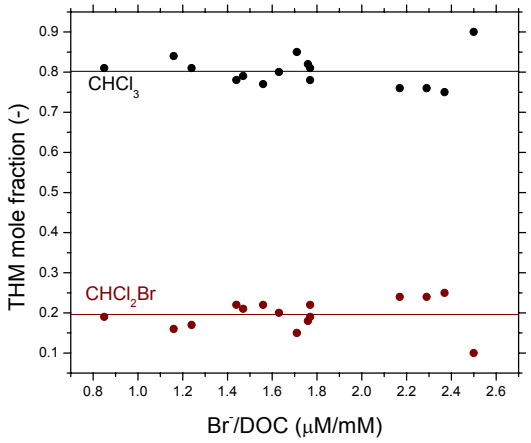

Figure 3.30. Effects of Br^-/DOC on mole fraction of THM species ($CHCl_3$ and $CHCl_2Br$)

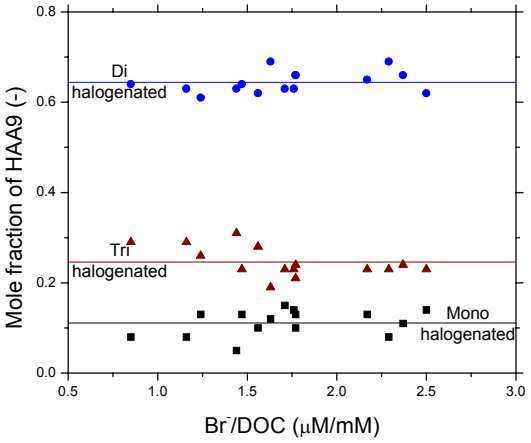

Figure 3.31. Effects of Br^-/DOC on mole fraction of mono-, di-, and trihalogenated HAAs.

Figures 3.30 depicts invariant mole fractions of the only two THM species that were present at concentrations greater than the method detection limit (1 μg/L). Mole fractions of monohalogenated (ClAA and BrAA), dihalogenated (Cl_2AA, Br_2AA, and BrClAA), and trihalogenated (Cl_3AA, Br_3AA,

$BrCl_2AA$, and Br_2ClAA) HAA species in permeate waters are depicted in Figure 3.31. In the range of experimental conditions investigated, the distribution of mono-, di-, and trihalogenated HAAs appeared to be independent of Br^-/DOC. The dihalogenated species constituted the largest mole fraction (~64%), followed by the trihalogenated species (~ 24%), and then the monohalogenated species (~11%) of the total HAAs on average. Cowman and Singer (41) have also reported invariant mole fractions of mono-, di-, and trihalogenated HAAs in humic acid extracts spiked with varying amounts of Br^-. However, the trihalogenated HAAs were the dominant species in their study. The invariant mole fractions of mono-, di-, and trihalogenated HAA species with changes in Br^-/DOC molar ratio suggests that the brominated HAAs are formed through the same mechanisms as the chlorinated ones.

3.11. Bromine Incorporation

One method of expressing the relative molar concentrations of brominated THM species is to calculate the bromine incorporation factor n, which quantifies the degree of bromine substitution (54):

$$n = \frac{\sum_{k=0}^{3} k \times [CHCl_{3-k}Br_k]}{\sum_{k=0}^{3} [CHCl_{3-k}Br_k]} \qquad (18)$$

Where each THM specie is expressed in μmol/L. This concept has been extended to define a HAA6 bromine incorporation factor (55). The bromine incorporation factor (n′) also provides a convenient method of quantifying the extent of bromine substitution into nine haloacetic acids (7).

$$n' = \frac{[MBAA]+[BCAA]+[BDCAA]+2\times[DBCAA]+2\times[DBAA]+3\times[TBAA]}{[MCAA]+[DCAA]+[TCAA]+[MBAA]+[BCAA]+[BDCAA]+[DBCAA]+[DBAA]+[TBAA]} \qquad (19)$$

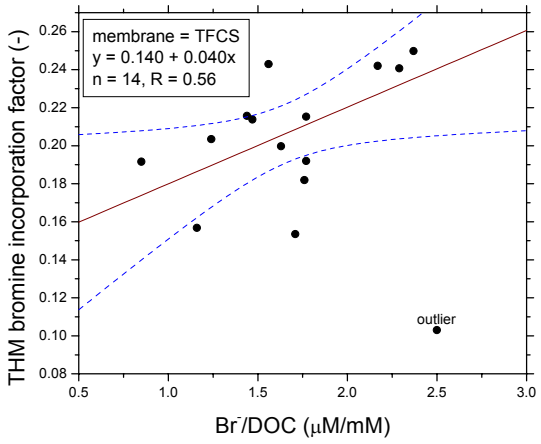

Figure 3.32. Effects of Br/DOC ratio on THM bromine incorporation factor.

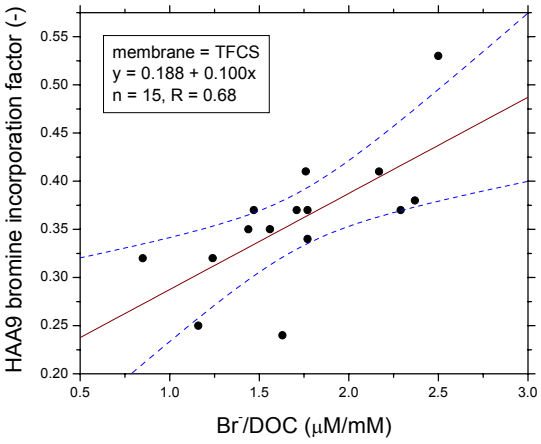

Figure 3.33. Effects of Br/DOC ratio on THM bromine incorporation factor.

Both n and n′ lie in the range [0, 3] and increase with the degree of bromine substitution. One NF membrane has been reported to increase n and n′ for HAA6 by a factor of 1.2 – 5.4 (5). Only one study has reported changes in n′ incorporating all nine HAAs upon nanofiltration (7). Because both bromide ion and dissolved organic carbon were both substantially removed by nanofiltration, using SUVA as the independent variable to study changes in bromine substitution into trihalomethanes and haloacetic acids is not appropriate. Figures 3.32 and 3.33 depict bromine incorporation into THMs and HAA9 respectively. As observed, bromine incorporation into both THMs and HAAs increased with increasing Br/DOC ratio.

The initial free chlorine concentration to dissolved organic carbon concentration was kept constant at 3.3 mg Cl_2 /mg DOC in the experiments reported herein. Under these conditions, the brominated THM and HAA species form first consuming the reactive precursor sites and in the process restricting formation of the chlorinated species because hypobromous acid is a stronger halogenating agent than hypochlorous acid (56). Thus, n and n′ increased with increasing Br^-/DOC ratio.

3.12. Bromide Utilization

Another method to quantify changes in bromine substitution is the concept of bromide utilization that was originally proposed for trihalomethanes (51). This concept can be extended to include HAAs:

$$\text{THM bromide utilization} = \frac{\sum_{i=1}^{3} i \times [CHCl_{3-i}Br_i]}{[Br^-]} \quad (20)$$

$$\text{HAA9 bromide utilization} = \frac{[MBAA] + 2[DBAA] + 3[TBAA] + [BrClAA] + [BrCl_2AA] + 2[Br_2ClAA]}{[Br^-]} \quad (21)$$

Where the concentrations are on a molar basis.

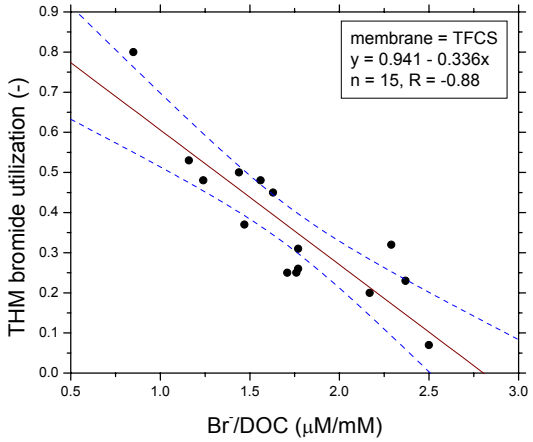

Figure 3.34. Effects of Br/DOC ratio on THM bromide utilization.

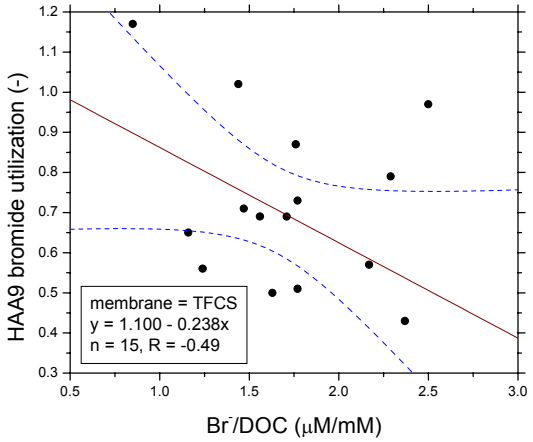

Figure 3.35. Effects of Br/DOC ratio on HAA bromide utilization.

Permeates that are limited with respect to natural organic matter possess very few sites for bromine substitution. Because hypobromous acid (HOBr) is a more powerful halogenating agent than hypochlorous acid (HOCl), the brominated DBPs are formed first with bromine consuming the available sites on NOM. In precursor limited permeates, bromide utilization is reduced because excess Br^- cannot react once available reactive sites on natural organic matter become occupied. Thus, decreasing bromide utilization observed in Figures 3.34 and 3.35 demonstrate that nanofilter permeate waters in this study were limited with respect to natural organic matter disinfection by-product precursors.

4. Quality Control and Quality Assurance

During the conduct of this research, various quality control (QC) measures were undertaken to ensure analytical precision and accuracy. The quality control measures include strict adherence to the methods described in the previous chapter, careful elimination of interferences from glassware, proper collection and storage of samples, regular maintenance of analytical equipments, duplicate and laboratory fortified matrix analysis of samples. The duplicate and spiked sample analyses were translated in statistical terms to evaluate the validity and accuracy of the data.

For sodium, chloride, and DOC, six calibration standards were employed; one each for lower and upper ranges and four proportionally divided throughout the middle of the expected range. At least two standards, one duplicate sample, and one spiked quality control sample was run at the end of every tenth sample and precision and accuracy analysis was done for each batch of ten sample. All standards were run at the end of the sample analysis. If the precision and accuracy of the analysis were outside the criteria, sample analysis was discontinued, the cause was determined and/or the instrument was recalibrated.

4.1. Precision

Precision was estimated by means of duplicate analyses. The results of duplicate analyses were used to calculate the relative percentage difference, RPD, as described in EPA Handbook for Quality Control in Water and Wastewater Laboratories (57). The RPD is defined as

$$RPD(\%) = \frac{(A-B)}{\frac{A+B}{2}} \times 100 \text{ where,}$$

RPD = Relative percentage difference

A = Duplicate value 1

B = Duplicate value 2.

The standard deviation (σ) is defined as

$$\sigma = \left(\frac{\sum_{i=1}^{n} \left(RPD_i - \overline{RPD} \right)^2}{n-1} \right)^{1/2}$$

Where,

$\overline{RPD}$ = mean of RPD

n = number of pairs of duplicate samples.

The average and standard deviation (σ) of this statistic were used to define the acceptable region for duplicate analyses. The upper control level and (UCL) and upper warning level (UWL) were established using following equations:

$$UCL = \overline{RPD} + 3\sigma$$

$$UWL = \overline{RPD} + 2\sigma$$

The values of RPD beyond UCL were assumed to be out of control and analysis was halted until the cause of non-compliance was ascertained and remedied. The values of RPD that exceeded two times the standard deviation were considered to be in the range of UWL. If the RPD values occurred in this range

then analytical procedure was reviewed for all possible errors, but analysis was not halted unless two subsequent results crossed the UWL.

Results of duplicate analysis for sodium are given in Table 4.1 along with the calculated relative percentage difference. The average value of RPD was determined to be 1.15%, indicating UWL and UCL to be 3.37% and 4.48%, respectively. Table 4.1 also shows that none of the eleven duplicate samples exceeded the UWL. Further, none of the duplicate samples analyzed exceeded the UCL indicating that the reproducibility in duplicate analyses was satisfactory.

Table 4.1. Precision Analysis of Sodium Duplicates.

Duplicate A (mg/L)	Duplicate B (mg/L)	RPD (%)
7.6	7.6	0.00
20.2	19.9	1.80
9.89	9.89	0.00
20.5	20.2	1.62
17.1	16.5	3.27
23.4	23.4	0.00
39.5	40.1	1.38
30.5	30.2	0.76
19.6	19.6	0.10
19.6	20.0	2.28
29.81	29.89	0.27

$\overline{RPD}$ = 1.15%

σ = 1.11%

UCL = 4.48%

UWL = 3.37%

Results for duplicate analyses for chloride are given in Table 4.2. The average value for RPD was 1.44%, and σ was 1.37%. The UWL and UCL were 5.55% and 4.18%, respectively. None of the duplicate samples seems to cross the UCL and UWL again suggesting that all analyses were satisfactory.

Table 4.2. Precision analysis of chloride duplicates.

Duplicate A (mg/L)	Duplicate B (mg/L)	RPD (%)
35.2	35.1	0.28
19.0	19.6	3.11
19.4	19.6	1.03
5.56	5.57	0.18
30.2	29.5	2.35
11.27	11.12	1.34

49.2	50.6	2.81
9.9	10.3	3.96
38.5	38.6	0.26
36.2	36.3	0.28
20.9	19.3	0.27

$\overline{RPD}$ = 1.44 %

σ = 1.37 %

UCL = 5.55 %

UWL = 4.18 %

Duplicate analyses for DOC are presented in Table 4.3. The average value for RPD was 4.60% having a σ of 3.99%. The UCL and UWL were 16.57% and 12.58%, respectively.

Table 4.3. Precision Analysis of DOC Duplicates.

Duplicate A (mg/L)	Duplicate B (mg/L)	RPD (%)
7.8	7.9	0.8
2.9	2.9	1.4
5.0	5.2	5.5
2.9	2.8	2.8
7.2	6.8	5.5
9.8	9.5	3.2
2.9	2.6	10.6
10.0	10.5	5.1
5.3	5.3	0.4
6.6	7.5	12.1
8.7	9.0	3.3

$\overline{RPD}$ = 4.60 %

σ = 3.99 %

UCL = 16.57 %

UWL = 12.58 %

4.2. Accuracy

To obtain accuracy of a particular analytical method, samples were spiked with a known concentration of analyte. These are referred to as spiked samples. The laboratory fortified sample matrix was prepared from a sample matrix, which was analyzed prior to fortification. Care was taken to make sure that fortified concentration was more than the observed background concentration of unfortified matrix. The results of spiked analyses were used to calculate the percent recovery (R), as described in EPA Handbook for Quality Control in Water and Wastewater Laboratories (57). The recovery is defined as:

$$R = \frac{C_s - C_u}{C_e} \times 100$$

Where,

R = percent recovery

C_s = fortified sample concentration

C_u = sample background concentration

C_e = expected concentration of spike in sample.

The standard deviation (σ) is defined as

$$\sigma = \left(\frac{\sum_{i=1}^{n} \left(R_i - \overline{R} \right)^2}{n-1} \right)^{1/2}$$

where,

$\overline{R}$ = mean of recovery

n = number of spiked samples.

The average and standard deviation (sd) of this statistic were used to define the acceptable region for duplicate analyses. The upper control level and (UCL) and upper warning level (UWL) were established using following equations:

$$UCL = \overline{R} + 3\sigma$$

$$UWL = \overline{R} + 2\sigma$$

The values of R above UCL were assumed to be out of control and analysis was halted until the cause of non-compliance was ascertained and remedied. The values of R that exceeded two times the standard deviation were considered to be in the range of UWL. If the R values occurred in this range then analytical procedure was reviewed for all possible errors, but analysis was not halted unless two subsequent results crossed the UWL.

Accuracy of sodium analyses, as measured by percentage recovery from spiked sample is shown in Table 4.4. The average recoveries were in the range of 96.2-106.7%.

Table 4.4. Accuracy analysis of sodium measured as percent recovery.

Spiked Value (mg/L)	Recovered Value (mg/L)	R (%)
23.1	24.7	106.7
26.2	25.6	97.8
30.0	32.0	106.7
32.7	34.4	105.0
25.7	25.6	99.4
28.3	27.9	98.7
31.4	30.2	96.2
34.5	34.4	99.8
43.0	42.2	98.1
15.9	15.8	99.5
15.6	16.4	105.3

R = 101.90 %

σ = 3.89 %

UCL = 113.57 %

UWL = 109.68 %

Accuracy of chloride measurements as calculated by percent recovery from spiked samples is shown in Table 4.5. The average percent recovery was 99.68% with σ of 2.97%.

Table 4.5. Accuracy Analysis of Chloride Measured as Percent Recovery

Spiked Value (mg/L)	Recovered Value (mg/L)	R (%)
41.6	42.3	101.8
29.8	28.4	95.3
45.5	43.3	95.1
30.0	30.3	100.7
35.6	34.8	97.7
33.8	33.1	98.1
41.9	41.4	98.7
33.9	34.5	101.8
32.5	32.7	100.5
34.4	35.9	104.5
29.7	30.4	102.3

R = 99.68 %

σ = 2.97 %

UCL = 108.60 %

UWL = 105.62 %

Results of recovery analyses for DOC analyses are shown in Table 4.6. The mean value for the percentage recovery was 102.80% and the σ was 6.66%. The UWL and UCL were 116.12% and

122.78%, respectively. None of the eleven spiked samples fell outside the UCL and UWL, indicating that the analytical method employed was appropriate.

Table 4.6. Accuracy analysis of DOC measured as percent recovery.

Spiked Value (mg/L)	Recovered Value (mg/L)	R (%)
8.9	9.3	104.2
8.6	8.4	97.9
3.4	3.9	112.9
10.1	10.3	102.1
15.1	13.3	88.0
6.5	7.0	108.7
6.4	6.4	98.9
16.5	17.6	106.4
16.8	18.0	107.0
15.9	15.8	99.5
15.6	16.4	105.3

R = 102.80 %

σ = 6.66 %

UCL = 122.78 %

UWL = 116.12 %

4.3. Assessing Surrogate Recovery

Surrogate is a pure analyte that is extremely unlikely to be found in any sample, and which is added to a sample aliquot in known amounts before extraction and is measured with the same procedures used to measure other sample components. The purpose of surrogate analysis is to monitor method performance with each sample. Deviation in surrogate recovery may indicate an extraction problem. The surrogate is a means of assessing method performance in every analysis from extraction to final chromatographic performance. As per EPA 552.1 for analysis to be accurate the surrogate recovery should be in the range of 70-130% and with 551.1 it is 80-120%.

Surrogate recovery was calculated as follows:

$$REC_S(\%) = \frac{Sam_{SR}}{Cal_{SR}} \times 100$$

REC_s (%) = Percentage surrogate recovery

Sam_{SR} = sample response

Cal_{SR} = mean surrogate response from the calibration standard analyses.

Tables 4.7 and 4.8 show the corresponding surrogate recoveries for THMs and HAAs analysis. More than 95% of the samples analyzed were within the limits specified by the EPA 552.1 and 551.1, indicating appropriate method performance. For THMs, surrogate analysis conducted on 2nd February 2001 showed inconsistencies in the surrogate recovery. One plausible reason could be inconsistent spiking of surrogate, which might have happened because of changes in trainee staff at the City of Houston East Water Purification Plant laboratory.

Table 4.7. Surrogate recovery analysis of THMs measured as percent recovery.

Date	Sample ID	Sample Surrogate Response	% Surrogate Recovery
02/12/01 (mean calibration response = 3.9546E+05)	31-feed	4.3052E+05	108.87
	5	5.2770E+05	133.44
	30	4.0928E+05	103.49
	50	4.8133E+05	121.71
	77	5.1904E+05	131.25
	90	4.5158E+05	114.19
	13-feed	3.3435E+05	84.55
	13-20	4.4037E+05	111.36
	13-16	4.8758E+05	123.30
	13-8	3.8728E+05	97.93
	18-feed	4.4504E+05	112.54
	18-25	5.3520E+05	135.34
	18-16	4.5447E+05	114.92
	18-8	5.2261E+05	132.15
	18-20	4.6257E+05	116.97
02/05/01 (mean calibration response = 2.7302E+05)	31-feed	4.3860E+05	160.65
	5	4.2451E+05	155.49
	30	3.7990E+05	139.15
	50	4.5535E+05	166.78
	77	3.0888E+05	113.14
	90	7.6146E+04	27.89
	13-feed	1.7709E+05	64.86
	13-20	2.9539E+05	108.20
	13-16	3.1757E+05	116.32
	13-8	2.6640E+05	97.57
	18-feed	3.1448E+05	115.19
	18-25	3.9524E+04	14.48
	18-16	9.9024E+04	36.27
	18-8	2.7470E+05	100.62
	18-20	3.2705E+05	119.79

Table 4.8. Surrogate recovery analysis of HAA measured as percent recovery.

Date	Sample ID	Sample Surrogate	% Surrogate Recovery

		Response	
02/12/01 (mean calibration response = 2.0962E+06)	31-feed	1.8467E+06	88.10
	5	1.5613E+06	74.48
	30	1.8740E+06	89.40
	50	1.7894E+06	85.37
	77	2.3218E+06	110.76
	90	1.5174E+06	72.39
	13-feed	1.7924E+06	85.51
	13-20	1.7199E+06	82.05
	13-16	2.1157E+06	100.93
	13-8	1.8054E+06	86.13
	18-feed	2.2202E+06	105.92
	18-25	1.8542E+06	88.45
	18-16	1.6299E+06	77.75
	18-8	1.4736E+06	70.30
	18-20	1.5755E+06	75.16
02/05/01 (mean calibration response = 2.1815E+06)	31-feed	2.2361E+06	102.50
	5	2.3486E+06	107.66
	30	2.3232E+06	106.49
	50	2.3717E+06	108.72
	77	1.9143E+06	87.75
	90	2.3011E+06	105.48
	13-feed	2.3310E+06	106.85
	13-20	2.0346E+06	93.26
	13-16	2.2174E+06	101.64
	13-8	2.6640E+05	12.21
	18-feed	2.3914E+06	109.62
	18-25	2.4781E+06	113.59
	18-16	1.7646E+06	80.89
	18-8	2.3130E+06	106.03
	18-20	2.2668E+06	103.91

4.4. Assessing the Internal Standard

The internal standard (IS) response (peak area) of all injections including calibration standards and samples were monitored through out the analysis. As per EPA 552.1, this response should not deviate more than 30% from its a mean IS response. Also as per EPA 551.1, this response should not deviate more than 20% from its mean IS response. Internal standard analyses data are tabulated in Tables 4.9 and

4.10 for THMs and HAAs, respectively. The results revealed that the percent error for all the samples were less than 20% from its mean response, indicating consistent GC performance during the analysis.

Table 4.9. Internal standard analysis of THMs measured as percent error.

Date	Sample ID	Sample Surrogate Response	% Error
02/12/01 (mean calibration response = 1.2176E+05)	31-feed	1.1551E+05	5.13
	5	1.0674E+05	12.33
	30	1.0827E+05	11.07
	50	1.1015E+05	9.53
	77	1.1009E+05	9.58
	90	1.0880E+05	10.64
	13-feed	1.0430E+05	14.34
	13-20	1.0276E+05	15.61
	13-16	1.0137E+05	16.74
	13-8	1.0169E+05	16.48
	18-feed	1.0833E+05	11.03
	18-25	1.0884E+05	10.61
	18-16	1.0551E+05	13.35
	18-8	1.0666E+05	12.40
	18-20	1.0341E+05	15.07
02/05/01 (mean calibration response = 8.0421E+04)	31-feed	8.6060E+04	7.01
	5	7.6042E+04	5.45
	30	6.3385E+04	21.18
	50	8.8077E+04	9.52
	77	8.1502E+04	1.34
	90	8.2361E+04	2.41
	13-feed	7.8001E+04	3.01
	13-20	8.1165E+04	0.92
	13-16	8.6278E+04	7.28
	13-8	8.1219E+04	0.99
	18-feed	8.0587E+04	0.21
	18-25	8.0057E+04	0.45
	18-16	8.5170E+04	5.90
	18-8	7.8629E+04	2.23
	18-20	8.7489E+04	8.79

Table 4.10. Internal standard analysis of HAAs measured as percent error

Date	Sample ID	Sample Surrogate Response	% Error
02/12/01 (mean calibration response = 5.2276E+05)	31-feed	5.2005E+05	0.52
	5	5.0931E+05	2.57
	30	5.4629E+05	4.50
	50	6.1491E+05	17.63
	77	5.8176E+05	11.29
	90	5.1322E+05	1.83
	13-feed	5.4411E+05	4.09
	13-20	5.0441E+05	3.51
	13-16	5.2446E+05	0.33
	13-8	4.6663E+05	10.74
	18-feed	5.9712E+05	14.23
	18-25	5.3043E+05	1.47
	18-16	5.2226E+05	0.09
	18-8	5.2730E+05	0.87
	18-20	5.0612E+05	3.18
02/05/01 (mean calibration response = 5.3183E+05)	31-feed	5.1080E+05	3.96
	5	5.1723E+05	2.75
	30	5.2040E+05	2.15
	50	5.3070E+05	0.21
	77	5.2274E+05	1.71
	90	5.2599E+05	1.10
	13-feed	5.1302E+05	3.54
	13-20	5.0810E+05	4.46
	13-16	5.0245E+05	5.53
	13-8	4.6663E+05	12.26
	18-feed	5.1934E+05	2.35
	18-25	5.3735E+05	1.04
	18-16	5.4891E+05	3.21
	18-8	5.1704E+05	2.78
	18-20	5.2224E+05	1.81

5. Summary of Principal Findings

Nonlinear fits of mass transfer coefficients to a simple closed form analytical expression suggests that both molecular weight and aqueous diffusion coefficients of contaminants influence their removal by nanofiltration membranes. Our approach to rejection calculations cannot be employed in a purely predictive mode for a multi-component system primarily because fundamental thermodynamic properties of contaminants encountered in water treatment have not yet been determined due to their heterogeneity as well as the complex composition of natural and pretreated feed waters. This is not surprising because, even mass transfer coefficients of single, fully dissociated ionic solutions are dependent on solute concentration (58) and are difficult to predict apriori. Complexation of inorganic ions with NOM, incomplete characterization of membrane and feed water composition, and unavailability of methods to identify dominant ion pairs encountered in water treatment (10) can be expected to further complicate rejection calculations from multi-solute solutions.

Even with this important limitation, the simplified model can quantitatively fit rejection of natural organic matter and DBP precursors by thin-film composite nanofiltration membranes. This result is consistent with the notion that molecular diffusion plays an important role in contaminant rejection even in NF membranes under conditions typical of water treatment. The model can also be employed to better interpret site-specific bench-, and pilot-scale experiments conducted in support of plant design.

Diffusion-dominated transport of NOM and DBP precursors may limit the upper bound of recovery and/or necessitate changes in the secondary disinfectant for highly colored waters to comply with anticipated Stage II DBP regulations. Thus, the design recovery in installations employing these new generation NF membranes in water treatment should be determined from considerations of concentrate disposal, precipitative fouling, as well as finished water quality.

Decreasing molar concentrations of THMs and HAA9 in permeates with increasing Br^-/DOC ratio suggests that nanofiltration produces waters that are limited with respect to organic precursors to DBPs. The invariant mole fractions of mono-, di-, and trihalogenated HAA species with changes in Br^-/DOC molar ratio suggests that the brominated HAAs are formed through the same mechanisms as the chlorinated ones.

Bromide utilization into THMs and HAAs decreased as permeate waters became increasingly precursor limited with increasing Br^-/DOC. However, bromine incorporation into THMs and HAAs increased in permeate waters with increasing Br^-/DOC because HOBr is a better halogenating agent compared to HOCl.

Excellent correlations obtained for TTHMs and HAA9 using DOC, UV_{254} and Cl_2 consumed as independent variables suggest that they all can be employed as DBP surrogates even in nanofiltered waters. Thus, simpler, more rapid, and cheaper measurements such as UV_{254}, DOC, and Cl_2 consumed can be employed as surrogates for aqueous DBP concentrations even in chlorinated nanofiltered waters.

THM yield decreased while HAA9 yield increased with Br^-/DOC. These data suggest that nanofiltration decreased reactivity of NOM with respect to THMs but increased its reactivity with respect to HAAs. Additional research is needed to confirm these findings.

Permeate molar HAA9 concentrations were always higher than THM molar concentrations presumably because Lake Houston water contained low concentrations of bromide ion. HAA9 concentration could be expected to have increased further if the DBP enumerations tests had been conducted at a pH lower than 8. Thus, current DBP regulations that limit HAA concentrations to lower levels than THM concentrations may need to be adjusted for low bromide waters chlorinated at near neutral pH values, health effects withstanding.

6. List of References

1. USEPA, *National Primary Drinking Water Regulations: Disinfectants and Disinfection By-Products; Final Rule*, 1998: Washington D.C. p. 69390-69476.
2. USEPA, *National Primary Drinking Water Regulations: Interim Enhanced Surface Water; Final Rule*, 1998, Environmental Protection Agency: Washington D.C. p. 69478 - 69521.
3. Lee, R.W. and W. Rast, *Light Attenuation in a Shallow, Turbid Reservoir, Lake Houston, Texas*, 1997, U.S.G.S. and City of Houston: Austin, TX. p. 33.
4. Chellam, S., *et al.*, *Jour. Am. Wat. Wks. Assn.,* Effect of Pretreatment on Surface Water Nanofiltration, (1997). **89**(10): p. 77-89.
5. Allgeier, S.C. and R.S. Summers, *Jour. Am. Wat. Wks. Assn.,* Evaluating NF for DBP Control with the RBSMT, (1995). **87**(3): p. 87-99.
6. Blau, T.J., *et al.*, *Jour. Am. Wat. Wks. Assn.,* DBP Control by Nanofiltration: Cost and Performance, (1992). **84**(12): p. 104-116.
7. Chellam, S., *Environ. Sci. Technol.,* Effects of Nanofiltration on Trihalomethane and Haloacetic Acid Precursor Removal and Speciation in Waters Containing Low Concentrations of Bromide Ion, (2000). **34**(9): p. 1813-1820.
8. Tan, L. and G.L. Amy, *Jour. Am. Wat. Wks. Assn.,* Comparing Ozonation and Membrane Separation for Color Removal and Disinfection By-Product Control, (1991). **83**(5): p. 74-79.
9. Soltanieh, M. and W.N. Gill, *Chem. Eng. Commun.,* Review of Reverse Osmosis Membranes and Transport Models, (1981). **12**: p. 279-363.
10. Marinas, B.J. and R.E. Selleck, *Jour. Memb. Sci.,* Reverse Osmosis Treatment of Multicomponent Electrolyte Solutions, (1992). **72**: p. 211-229.
11. Matsuura, T., *Synthetic Membranes and Membrane Separation Processes*. 1993, Boca Raton, FL: CRC Press.
12. USEPA, *ICR Manual for Bench- and Pilot-Scale Treatment Studies*, . 1996, Office of Ground Water and Drinking Water: Cincinnati, OH. p. 1-1 - 3-108.
13. Rosa, M.J. and M.N. de Pinho, *Jour. Memb. Sci.,* Separation of Organic Solutes by Membrane Pressure-Driven Processes, (1994). **89**: p. 235-243.
14. van der Bruggen, B., *et al.*, *Jour. Memb. Sci.,* Influence of Molecular Size, Polarity, and Charge on the Retention of Organic Molecules by Nanofiltration, (1999). **156**: p. 29-41.
15. Amy, G.L., *et al.*, *Jour. Am. Wat. Wks. Assn.,* Comparing Gel Permeation Chromatography and Ultrafiltration for the Molecular Weight Characterization of Aquatic Organic Matter, (1987). **79**(1): p. 43-49.
16. Chin, Y.-P., *et al.*, *Environ. Sci. Technol.,* Molecular Weight, Polydispersivity, and Spectroscopic Properties of Aquatic Humic Substances, (1994). **28**(11): p. 1853-1858.
17. Croue, J.-P., *et al.*, *Natural Organic Matter: Structural Characteristics and Reactive Properties*, in *Formation and Control of Disinfection By-Products in Drinking Water*, P.C. Singer, Editor. 1999, AWWA: Denver, CO. p. 65-93.
18. Cho, J., *et al.*, *Water Research,* Membrane Filtration of Natural Organic Matter: Initial Comparison of Rejection and Flux Decline Characteristics with Ultrafiltration and Nanofiltration Membranes, (1999). **33**(11): p. 2517-2526.

19. Hong, S. and M. Elimelech, *Jour. Memb. Sci.,* Chemical and Physical Aspects of Natural Organic Matter Fouling of Nanofiltration Membranes, (1997). **132**: p. 159-181.

20. Lonsdale, H.K., *et al.*, *Jour. Appl. Poly. Sci.,* Transport Properties of Cellulose Acetate Osmotic Membranes, (1965). **9**: p. 1341-1362.

21. Chellam, S. and J.S. Taylor, *Wat. Res.,* Simplified Analysis of Contaminant Rejection During Ground- and Surface Water Nanofiltration Under the Information Collection Rule, (2001). **35**(10): p. 2460-2474.

22. Taylor, J.S. and E.P. Jacobs, *Reverse Osmosis and Nanofiltration*, in *Water Treatment Membrane Processes*, J. Mallevialle, P.E. Odendaal, and M.R. Wiesner, Editors. 1996, McGraw Hill: New York, N.Y. p. 9.1-9.70.

23. Lonsdale, H.K., *Theory and Practice of Reverse Osmosis and Ultrafiltration*, in *Industrial Processing with Membranes*, R.E. Lacey, and Loeb, S., Editor. 1979, Robert E. Krieger Publishing Company: Huntington, N.Y. p. 123-178.

24. Jonsson, G. and C.E. Boesen, *Polarization Phenomena in Membrane Processes*, in *Synthetic Membrane Processes: Fundamentals and Water Applications*, G. Belfort, Editor. 1984, Academic Press, Inc.: New York, N.Y. p. 101-130.

25. van den Berg, G.B., *et al.*, *Jour. Memb. Sci.,* Mass Transfer Coefficients in Ultrafiltration, (1989). **47**: p. 25-51.

26. Sourirajan, S., *Reverse Osmosis*. 1970, New York, N.Y.: Academic Press. 580.

27. Wiesner, M.R. and C.A. Buckley, *Principles of Rejection in Pressure-Driven Membrane Processes*, in *Water Treatment Membrane Processes*, J. Mallevialle, P.E. Odendaal, and M.R. Wiesner, Editors. 1996, McGraw Hill: New York, N.Y. p. 5.1-5.17.

28. Press, W.H., *et al.*, *Numerical Recipes in FORTRAN: The Art of Scientific Computing*. 2nd ed. 1992, New York, N.Y.: Cambridge University Press. 963.

29. Dennis, J.E., *et al.*, *ACM Trans. Math. Soft.,* An Adaptive Nonlinear Least-Squares Algorithm, (1981). **7**(3): p. 348-368.

30. Bates, D.M. and D.G. Watts, *Nonlinear Regression Analysis and Its Applications*. 1988, New York, N.Y.: John Wiley & Sons.

31. Watts, D.G., *The Canadian Journal of Chemical Engineering,* Estimating Parameters in Non-Linear Rate Equations, (1994). **72**: p. 701-710.

32. Lyman, W.J., *et al.*, *Handbook of Chemical Property Estimation Methods: Environmental Behavior of Organic Compounds*. 1981, New York, N.Y.: McGraw-Hill Book Company.

33. Hautman, D.P. and D.J. Munch, *EPA Method 300.1: Determination of Inorganic Anions in Drinking Water by Ion Chromatography, Revision 1.0*, 1997, U.S. EPA: Cincinnati, OH.

34. Summers, R.S., *et al.*, *Jour. Am. Wat. Wks. Assn.,* Assessing DBP Yield: Uniform Formation Conditions, (1996). **88**(6): p. 80-93.

35. Munch, D.J., *et al.*, *Method 552.2: Determination of Haloactetic Acids and Dalapaon in Drinking Water by Liquid Liquid Extraction, Derivatization, and Gas Chromatography with Electron Capture Detection, Revision 1.0*, 1995, EPA, National Exposure Research Laboratory: Cincinnati, OH.

36. Munch, D.J., *et al.*, *Method 551.1: Determination of Chlorination Disinfection By-Products, Chlorinated Solvents, and Halogenated Pesticides/Herbicides in Drinking Water by Liquid*

Liquid Extraction and Gas Chromatography with Electron-Capture Detection, Revision 1.0, 1995, U.S. EPA: Cincinnati, OH.

37. Chellam, S. and J.G. Jacangelo, *Jour. Environ. Eng.,* Existence of Critical Recovery and Impacts of Operational Mode on Potable Water Microfiltration, (1998). **124**(12): p. 1211-1219.

38. Lozier, J.C., *et al.*, *Jour. Am. Wat. Wks. Assn.,* Integrated Membrane Treatment in Alaska, (1997). **89**(10): p. 50-64.

39. Taniguchi, M. and S. Kimura, *AIChE Journal,* Estimation of Transport Parameters of RO Membranes for Seawater Desalination, (2000). **46**(10): p. 1967-1973.

40. Pourmoghaddas, H., *et al.*, *Jour. Am. Wat. Wks. Assn.,* Effect of Bromide Ion on Formation of HAAs During Chlorination, (1993). **85**(1): p. 82-87.

41. Cowman, G.A. and P.C. Singer, *Environ. Sci. Technol.,* Effect of Bromide Ion on Haloacetic Acid Speciation Resulting from Chlorination and Chloramination of Aquatic Humic Substances, (1996). **30**(1): p. 16-24.

42. Wu, W.W. and P.A. Chadik, *Jour. Environ. Eng.,* Effect of Bromide Ion on Haloacetic Acid Formation During Chlorination of Biscayne Aquifer Water, (1998). **124**(10): p. 932-938.

43. Singer, P.C., *et al.*, *Jour. Am. Wat. Wks. Assn.,* Trihalomethane Formation in North Carolina Drinking Waters, (1981). **72**(8): p. 392-401.

44. Singer, P.C. and S.D. Chang, *Jour. Am. Wat. Wks. Assn.,* Correlations Between Trihalomethanes and Total Organic Halides Formed During Water Treatment, (1989). **81**(8): p. 61-65.

45. Krasner, S.W., *et al.*, *Jour. Am. Wat. Wks. Assn.,* The Occurrence of Disinfection By-Products in US Drinking Water, (1989). **81**(8): p. 41-53.

46. Singer, P.C., *et al.*, *Jour. Am. Wat. Wks. Assn.,* DBPs in Chlorinated North Carolina Drinking Waters, (1995). **87**(10): p. 83-92.

47. Edzwald, J.K., *et al.*, *Jour. Am. Wat. Wks. Assn.,* Surrogate Parameters for Monitoring Organic Matter and THM Precursors, (1985). **77**(4): p. 122-132.

48. Najm, I.N., *et al.*, *Jour. Am. Wat. Wks. Assn.,* Evaluating Surrogates for Disinfection By-Products, (1994). **86**(6): p. 98-106.

49. Singer, P.C., *Jour. Environ. Engrg.,* Control of Disinfection By-Products in Drinking Water, (1994). **120**(4): p. 727-744.

50. Minear, R.A. and J.C. Bird, *Trihalomethanes: Impact of Bromide Ion Concentration on Yield, Species Distribution, Rate of Formation, and Influence of Other Variables*, in *Water Chlorination: Environmental Impact and Health Effects*, R.L. Jolley, W.A. Brungs, and R.B. Cumming, Editors. 1980, Ann Arbor Science: Ann Arbor, MI. p. 151-160.

51. Symons, J.M., *et al.*, *Jour. Am. Wat. Wks. Assn.,* Measurement of THM and Precursor Concentrations Revisited: The Effect of Bromide Ion, (1993). **85**(1): p. 51-62.

52. Krasner, S.W., *et al.*, *Jour. Am. Wat. Wks. Assn.,* Quality Degradation: Implications for DBP Formation, (1994). **86**(6): p. 34-47.

53. Dickenson, E.R.V. and G.L. Amy, *Natural Organic Matter Characterization of Clarified Waters Subjected to Advanced Bench-Scale Treatment Processes*, in *Natural Organic Matter and Disinfection By-Products: Characterization and Control in Drinking Water*, S.E. Barrett, S.W. Krasner, and G.L. Amy, Editors. 2000, American Chemical Society: Washington DC. p. 122-138.

54. Gould, J.P., *et al.*, *Formation of Brominated Trihalomethanes: Extent and Kinetics*, in *Water Chlorination: Environmental Impact and Health Effects*, R.L. Jolley, *et al.*, Editors. 1983, Ann Arbor Science Publishers: Ann Arbor, MI. p. 297-310.

55. Shuikary, H.M., *et al.*, *Jour. Am. Wat. Wks. Assn.,* (1994). **86**(6): p. 72-87.

56. Symons, J.M., *et al.*, *Influence of Bromide Ion on Trihalomethane and Haloacetic Acid Speciation*, in *Disinfection By-Products in Water Treatment: The Chemistry of their Formation and Control*, R. Minear and G.L. Amy, Editors. 1996, Lewis Publishers: Boca Raton, FL. p. 91-130.

57. USEPA, *Handbook for Analytical Quality Control in Water and Wastewater Laboratories*, . 1979, EPA Analytical Quality Control Laboratory: Cincinnati, OH.

58. Eriksson, P., *Jour. Memb. Sci.,* Water and Salt Transport Through Two Types of Polyamide Composite Membranes, (1988). **36**: p. 297-313.

7. Articles in Refereed Scientific Journals

Chellam, S., and Taylor, J.S., 2001. *Simplified Analysis of Contaminant Rejection During Ground- and Surface Water Nanofiltration Under the Information Collection Rule.* Water Research, **35** (10) 2460.

Chellam, S. and Krasner, S.W. *Disinfection By-Product Relationships and Speciation in Chlorinated Nanofiltered Waters.* Submitted to Environmental Science and Technology. 2001

Chellam, S. Chen, D-T, Francis, D.J. *Effects of Source Water Location, Season, and Membrane Type on Nanofilter Permeate water Quality.* Submitted to Environmental Engineering Science. 2001

8. Book Chapters

None

9. Dissertations

The research of one doctoral student (Ramesh Sharma) and a masters student (Grishma Shetty) have been partially supported by these funds. Their theses will be written in the near future.

10. Water Resources Research Institute Reports

None

11. Conference Proceedings

Chellam, S. *Disinfection By-Product Precursor Removal by Nanofiltration.* Paper in Research Session "Disinfection Using Membranes" Mon10. In American Water Works Association Annual Conference and Exposition, June 11 – 15, 2000, Denver, CO.

Sharma, R. and Chellam, S. *Effect of Process Variables on Membrane Molecular Weight Cut Off Determination and Implications for NOM Rejection by Nanofiltration.* Paper in Research Session III "Pretreatment Studies" T5. In American Water Works Association Membrane Technology Conference, March 4 – 7, 2001, San Antonio TX.

Chellam, S. *Quantifying Diffusion Limited Disinfection By-Product Precursor Transport Across Nanofiltration Membranes.* Paper in Research Session I "Water Quality" M5. In American Water Works Association Membrane Technology Conference, March 4 – 7, 2001, San Antonio TX.